Ore Geology Reviews xxx (xxxx) xxx–xxx

Contents lists available at ScienceDirect

Ore Geology Reviews

journal homepage: www.elsevier.com/locate/oregeorev

Low temperature alteration of magmatic Ni-Cu-PGE sulfides as a source for hydrothermal Ni and PGE ores: A quantitative approach using automated mineralogy

David A. Holwell[a,*], Zeinab Adeyemi[a,b], Laura A. Ward[a,b], Daniel J. Smith[a], Shaun D. Graham[b], Iain McDonald[c], Jennifer W. Smith[a,d]

[a] Department of Geology, University of Leicester, University Road, Leicester LE1 7RH, UK
[b] Carl Zeiss Microscopy Ltd, 509 Coldhams Lane, Cambridge CB1 3JS, UK
[c] School of Earth and Ocean Sciences, Cardiff University, Park Place, Cardiff CF10 3AT, UK
[d] Geological Survey of Canada, 601 Booth Street, Ottawa, On K1A 0E8, Canada

ARTICLE INFO

Keywords:
Magmatic sulfide
Alteration
Automated mineralogy
Ni-Cu-PGE
Hydrothermal Ni

ABSTRACT

Magmatic Ni-Cu-PGE sulfide assemblages are almost ubiquitously comprised of pyrrhotite-pentlandite-chalcopyrite(-pyrite). Sulfide alteration is common during syn- or post-magmatic fluid interaction, usually replacing sulfides with amphiboles or serpentine. However, some are altered to a low temperature (< 200 °C) hydrothermal assemblage of pyrite-millerite-chalcopyrite (PMC). An example is the Ni-Cu-PGE mineralisation in the Grasvally-Norite-Pyroxenite-Anorthosite (GNPA) Member, northern Bushveld Complex, which displays a continuum of mineralogical styles formed through progressive alteration: Style 1 primary pyrrhotite-pentlandite-chalcopyrite; which is altered to Style 2 pyrrhotite-pyrite-pentlandite-chalcopyrite; Style 3 pyrite-pentlandite-chalcopyrite; Style 4 pyrite-pentlandite-millerite-chalcopyrite; and Style 5 pyrite-millerite-chalcopyrite-cubanite. Modelling using CHILLER confirms this mineralogical sequence is thermodynamically possible at ~200 °C. Quantitative characterisation using automated Energy-Dispersive X-ray spectroscopy mapping alongside in situ laser ablation analyses determined mineral proportions, major and trace element concentrations and deportments in each style. The early loss of pyrrhotite removes over half of the bulk Fe and S during the initial stages of PMC alteration, increasing Cu, Ni and PGE tenors of the remaining sulfides significantly. As water–rock interaction progresses, pyrrhotite is replaced by pyrite and pentlandite by millerite, with concurrent losses in Fe, S and Ni. Copper is lost throughout the alteration, and is most pronounced in the more advanced stages. The fluids responsible were most likely acidic and oxidised, with metals mobilised as chloride complexes. Using Rh as an immobile normalising element, the overall mass loss in the most altered samples is calculated to be up to 90%, consistent with textural relationships that indicate 40–90% volume loss from Styles 2–5, with sulfides replaced by secondary silicates, including phlogopite, quartz, chlorite, pyroxenes and minor amphiboles. Magnetite is not a significant alteration product and thus Fe is mobilised, or incorporated into silicates. Most trace elements present in the magmatic sulfide (the IPGE, Rh and Bi) remain in the sulfide phases, and are effectively transferred to pyrite during PMC alteration, except Pd, which remains in pentlandite, and is liberated from the sulfide assemblage when pentlandite disappears. Selenium tenors increase slightly with alteration, demonstrating that alteration decreases S/Se ratios. The significant mobilisation of Ni, Cu and Pd during PMC alteration produces fluids enriched in these elements that may represent a metal source for a number of enigmatic hydrothermal Ni deposits such as Avebury, Enterprise and Talvivaara, whose metal sources remain speculative. The PMC alteration of the GNPA Member may be specifically a source for the nearby Waterberg hydrothermal Pt deposit. Furthermore, this study has implications not only for magmatic ore deposits, but also for the general implications of sulfide transformation and metal transfer in ore systems in general.

* Corresponding author.
E-mail address: dah29@le.ac.uk (D.A. Holwell).

http://dx.doi.org/10.1016/j.oregeorev.2017.08.025
Received 15 June 2017; Received in revised form 20 July 2017; Accepted 14 August 2017

1. Introduction

Magmatic sulfide deposits are the world's most important source of Ni and platinum-group elements (PGE) and significant associated Cu. They form following the segregation of an immiscible sulfide liquid from a mafic-ultramafic magma, with chalcophile elements being concentrated in the sulfide liquid, which accumulate into economic deposits (Naldrett, 2011). Cooling of the sulfide liquid crystallises Ni-rich monosulfide solide solution (mss) and Cu-rich intermediate solid solution (iss), which exsolve at low temperatures to give rise to the characteristic pyrrhotite–pentlandite–chalcopyrite sulfide assemblage that occurs in almost all unaltered magmatic sulfide ores (Craig and Kullurud, 1969; Kullerud et al., 1969).

Hydrothermal deposits of Ni sulfides and PGE are much less common but do exist, with Ni deposits found in mafic-ultramafic igneous, and sedimentary host rocks (González-Álvarez et al., 2013), and epigenetic PGE deposits found in a range of settings (Wood, 2002). These enigmatic classes of deposits include some major deposits, such as the Avebury Ni deposit, Tasmania, Australia (Keays and Jowitt, 2013), the Enterprise Ni deposit in Zambia's Copperbelt (Capistrant et al., 2015), the Waterberg hydrothermal Pt deposit in northern South Africa (McDonald et al., 1995), the hydrothermally remobilised Pt-Cu-Au New Rambler deposit, Wyoming (Nyman et al., 1990), and epigenetic Pt-Au deposits in Brazil and Australia (Sener et al., 2002). The source of metals in all these deposits is very poorly constrained but the most commonly proposed theory is that the metals have been mobilised from magmatic sulfides within mafic-ultramafic rocks, though no definitive evidence has been put forward and this key aspect of ore genesis remains speculative.

Alteration of magmatic sulfides is very common, and whilst Cu and Au are relatively mobile during fluid alteration, Ni and the PGE are generally thought to be immobile under most conditions, such as serpentinisation, amphibolitisation and talc-carbonate alteration of ultramafic rocks (e.g. Barnes and Liu, 2012). However, Liu et al. (2012) showed experimentally that Ni can become mobile in certain oxidised and acidic conditions and Le Vaillant et al. (2015, 2016a) have shown that there are other hydrothermal conditions that effectively mobilise Ni, Cu and PGE, such as those involving As-rich orogenic fluids. Effective mobilisation of Ni, Cu and PGE could produce fluids that are enriched in these elements and provide a source for enigmatic hydrothermal occurrences of this element association.

Replacement of magmatic sulfides by secondary silicates is extremely common, and usually takes the form of amphiboles such as actinolite-tremolite-talc around the margins of sulfide blebs (Li et al., 2004). This process generally reduces the volume of the sulfides slightly by replacing them from the outer edges. Whilst the sulfides are affected by this alteration, platinum-group minerals (PGM) are often left unaltered as satellite grains around the reduced sulfide grains (e.g. Hutchinson and Kinnaird, 2005). Nevertheless, the assemblages of such altered ores are still overwhelmingly dominated by pentlandite-pyrrhotite-chalcopyrite. However, there are a number of cases where low-temperature hydrothermal alteration has apparently changed the mineralogy of the sulfides, with pyrrhotite being altered to pyrite, pentlandite to millerite, and chalcopyrite being partially altered to cubanite (e.g. Dare et al., 2011; Djon and Barnes, 2012; Smith et al., 2011; Piña et al., 2012). This characteristic assemblage produces a more complex mineralogy, and PGE are either mobilised into the fluid phase, taken up variably by the secondary sulfide alteration products, or recrystallized as secondary PGM. As such, pyrite and millerite in such ores can become major hosts for Pt and other PGE (e.g. Oberthür et al., 1997; Barkov et al., 1997; Gervilla and Kojonen, 2002; Djon and Barnes, 2012; Dare et al., 2011; Piña et al., 2012, 2013; Smith et al., 2014; Graham et al., 2017).

Whilst this alteration of magmatic sulfides has been observed empirically, the transformation from a magmatic pentlandite-pyrrhotite-chalcopyrite assemblage to one of hydrothermal pyrite-millerite-chalcopyrite(–cubanite) has never been assessed quantitatively. The conversion of pyrrotite (Fe_7S_8) to pyrite (FeS_2) implies a relative gain of S; quite possible if a S-bearing fluid is involved in alteration. Alternatively, it could be a result of a loss of Fe, which would also be consistent with pentlandite ($(Fe,Ni)_9S_8$) converting to millerite (NiS); the latter also requiring some loss of Ni. Alteration of chalcopyrite ($CuFeS_2$) to cubanite ($CuFe_2S_3$) involves loss of Cu relative to S and Fe (possibly due to Fe gain), but also an increase in Fe relative to S. As such, the reactions in this style of alteration clearly involve significant changes in mineralogy; which will have a major impact on the ratios of the major constituents of the sulfide assemblage, the metal tenors of the sulfide, and the potential mobilisation of the base and precious metals into hydrothermal fluids. Determining whether mass loss or gain has occurred requires a quantitative approach with well-defined end members.

In this paper, we aim to quantify the hydrothermal alteration of magmatic pyrrhotite-pentlandite-chalcopyrite ores to pyrite-millerite-chalcopyrite assemblages (henceforth referred to as 'PMC alteration') by applying automated mineralogy, with supporting Laser Ablation-Inductively Coupled Plasma-Mass Spectrometry (LA-ICP-MS) data, to track the distribution and deportment of major and trace metals during PMC alteration. We utilise a suite of ore samples from the northern Bushveld Complex that show a continuum from unaltered, primary magmatic pentlandite-pyrrhotite-chalcopyrite to completely altered millerite-pyrite-chalcopyrite-cubanite. For the first time, we are able to quantify the process in terms of significant, but relatively variable bulk losses of Fe, Ni, Cu, PGE, Se and S from sulfide, major sulfide volume reduction, and the subsequent increase in the tenor of a number of base and precious metals. The significance of identifying effective Ni-Cu-PGE mobility and the implications of producing Ni-Cu-PGE-bearing hydrothermal fluids as a source for enigmatic hydrothermal deposits, and the wider processes of sulfide alteration and metal transfer in ore deposits, is explored.

2. Empirical and experimental studies

A number of magmatic sulfide deposits have been identified as comprising variable amounts of the low temperature assemblage of pyrite-millerite-chalcopyrite, usually as partial replacement of the primary pyrrhotite-pentlandite-chalcopyrite assemblage. These include deposits and occurrences in the northern Bushveld Complex, South Africa (Smith et al., 2011, 2014), the Lac Des Iles Complex, Canada (Djon and Barnes, 2012; Duran et al., 2015), Aguablanca, Spain (Piña et al., 2012), and the Great Dyke of Zimbabwe (Piña et al., 2016). In all of these studies, the presence of pyrite and millerite is attributed, at least in part, to low-temperature hydrothermal alteration, supported by textural relationships and the experimental evidence that the pyrite-millerite assemblage can only coexist at temperatures below around 230 °C (Naldrett and Kullerud, 1967; Naldrett et al., 1967; Craig, 1973; Misra and Fleet, 1974).

Both millerite and pyrite can however, form as a product of primary magmatic mss. In the case of millerite this is only in some cases of extremely Ni-enriched komatiite ores, in which Ni-rich mss can dissociate to assemblages of pyrite, pentlandite and millerite (Barnes et al., 2011). However, in all the cases of millerite in the more mafic systems cited above, it forms as an alteration product from pentlandite. Pyrite can also be a primary product of the cooling of mss if the S to metal ratio of the sulfide liquid is high enough (~40 wt% S at 600 °C), and up to 30% pyrite can be accommodated by a the breakdown of mss at temperatures below 700 °C (Naldrett et al. 1967; Kullerud et al. 1969; Craig 1973). Pyrite and pentlandite, however, cannot co-exsolve until 230 °C when the mss tie line separating pyrite and pentlandite in the Fe-Ni-S system breaks (Naldrett et al., 1967). Pyrite formed in the mss-iss-pyrite system has been shown experimentally to be enriched in a range of highly siderophile and chalcophile elements, such as the PGE, Te, Se and As (Cafagna and Jugo, 2016). However, most natural sulfide melts

do not contain such high proportions of S and so this process is relatively uncommon (Piña et al., 2016). Typically, the textures of primary pyrite formed from the breakdown of mss are distinctly euhedral and have contents of IPGE and Rh dependant on the initial concentrations of the mss constituents (Dare et al., 2011; Duran et al., 2015; Piña et al., 2016). Pyrite formed from hydrothermal alteration has a much more amorphous texture and carries very variable IPGE and Rh, though can contain significant, ppm-level, concentrations of Pt (Dare et al., 2011; Smith et al., 2014; Graham et al., 2017). In this paper, we focus entirely on the products of low temperature alteration.

3. The Grasvalley-Norite-Pyroxenite-Anorthosite member as a case study

The Grasvalley-Norite-Pyroxenite-Anorthosite (GNPA) member is located in the northern limb of the Bushveld Complex, South Africa, and is made up of a thick (400–800 m) package of layered ultramafic-mafic rocks that are equivalent in stratigraphic position to the Platreef to the north, and to the Merensky Reef in the Critical Zone of the eastern and western limbs of the Complex (Hulbert, 1983; Smith et al., 2011; Smith et al., 2014; Smith et al., 2016). The floor rocks are made up of metasedimentary quartzites and calc-silicates of the Pretoria Group of the Proterozoic Transvaal Supergroup; and Lower zone cumulates of the Bushveld Complex. Full details of the petrology, mineralogy, geochemistry and S isotope characteristics of the GNPA member can be found in Smith et al. (2011, 2014, 2016). Critically for this study, the GNPA member hosts disseminated, blebby sulfide mineralisation that displays the full continuum through the range of sulfide assemblages produced by the low temperature alteration of a primary magmatic assemblage of pyrrhotite-pentlandite-chalcopyrite to one containing pyrite-millerite-chalcopyrite (Smith et al., 2011; Sutherland et al., 2012; Adeyemi et al., 2016).

4. Sampling and methodology

This work utilises samples of quarter core obtained from boreholes drilled by Falconbridge Ltd and Caledonia Mining on the farms Rooipoort, Grasvally, Moorddrift and by Platinum Group Metals on War Springs. Further details, including core logs and maps can be found in Smith et al. (2011, 2014, 2016). Thin sections used by Smith et al. (2011) were re-examined at the ZEISS Natural Resources Laboratory, Cambridge, UK, using a ZEISS Axio Imager Z2m microscope with a 130 × 85 STEP (D) automated stage coupled with an AxioCamM3 camera to produce high resolution mosaic photographs in transmitted and reflected light. Nine sections containing a representative spread of sulfide assemblages through the alteration styles were selected for quantitative mineralogy at ZEISS. Samples were mapped using the Mineralogic software and petrological analyser. A ZEISS Sigma VP field emission Scanning Electron Microscope (SEM) was used, coupled with two Bruker 6|30 Energy Dispersive X-ray (EDX) Spectroscopy detectors. Counts for EDX detection were consistently above 3000 (in accordance with ZEISS' QA/QC) with mineral classifications based on stoichiometric values (wt%). Energy-dispersive X-ray spectroscopy calibrations were performed every hour on a Cu standard to normalise the beam alongside a brightness and contrast calibration to help limit the effects of beam drift. Analysis was undertaken using a step size of 5 µm whilst mapping, with an accelerating voltage of 20 kV, a working distance of 8.5 mm and dwell time of 0.0025 s. All sulfides and magnetite were included in the dataset. The use of Mineralogic gives quantitative modal mineralogy and elemental deportment data. A schematic workflow for the Mineralogic analysis is shown in Fig. 1.

The EDX mapping quantified the major sulfide phases and associated magnetite. In order to add trace element data to each sulfide phase we utilised the in situ laser ablation-inductively coupled plasma-mass spectrometry (LA-ICP-MS) of sulfide data from the GNPA member from Smith (2014); with summary data given in Smith et al. (2014),

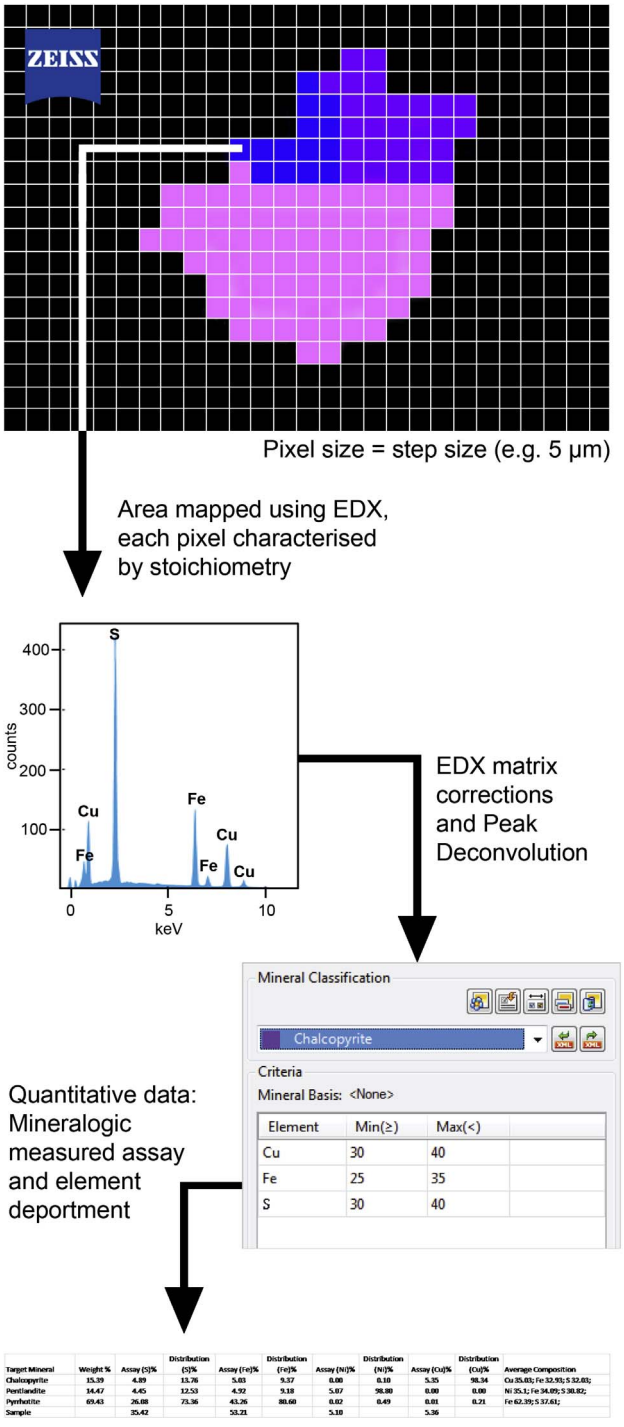

Fig. 1. Schematic representation of ZEISS' Mineralogic workflow.

which utilised the same samples. All conditions of the LA-ICP-MS analysis can be found in Prichard et al. (2013) and Smith et al. (2014).

Hydrothermal modification of the initial assemblage was modelled using an equilibrium reaction path model in the CHILLER code (Reed, 1982, 1998), with the SOLTHERM.H08 database (Reed and Palandri, 2013). This database includes equilibrium constants calculated with SUPCRT92 (Johnson et al., 1992); thermodynamic data from Holland and Powell (1998) and Shock (2007). Mineral solid solutions are represented by end-member compositions that are mixed using an ideal multisite mixing scheme. The model progresses by titration of rock into a synthetic hydrothermal fluid. The fluid was produced within the model by taking a typical seawater composition and increasing the

temperature to 200 °C, fractionating any minerals that saturate (e.g. calcite, anhydrite). As seawater is a mature fluid with respect to water-rock reaction, this synthetic fluid provides a range of anions and cations in appropriate concentrations to model generic hydrothermal alteration (rather than strongly fluid-buffered alteration by a fluid with extreme pH or chemistry). A mineral assemblage of 47.5 wt% anorthite, 28.5 wt % diposide, 19 wt% enstatite, 3 wt% pyrrhotite, 1 wt% pentlandite and 1 wt% chalcopyrite (based on mineralogy presented by Smith et al., 2011) was titrated into 1 kg of the fluid. Variable increment sizes were used to avoid non-convergence of calculations during periods of multiple mineral saturation / undersaturation. All precipitated minerals were capable of back-reacting with the fluid. All steps were carried out a temperature of 200 °C and pressures in excess of vapour saturation.

5. Textural analysis

Smith et al. (2011, 2014, 2016) discriminated between 'primary' (pyrrhotite-pentlandite-chalcopyrite) and 'secondary' (pyrite- and millerite-bearing) assemblages. Here we show that the sulfides show a continuum of mineral assemblages that can be split into five styles determined by the appearance or disappearance of certain sulfide phases (Fig. 2):

- Style 1: primary pentlandite-pyrrhotite-chalcopyrite
- Style 2: pentlandite-pyrrhotite-pyrite-chalcopyrite (pyrite appears)
- Style 3: pentlandite-pyrite-chalcopyrite (pyrrhotite disappears)
- Style 4: pentlandite-millerite-pyrite-chalcopyrite (millerite appears)
- Style 5: millerite-pyrite-chalcopyrite-cubanite (pentlandite disappears)

We refer to these as 'styles' rather than 'stages' as we consider the alteration to be a single event, rather than a multi-stage process. The assemblages listed above are representative of rocks that have been subject to a single episode of alteration, but that display increasing amounts of water-rock interaction. Fig. 2 shows backscattered electron images, Mineralogic phase maps, and reflected light microscopy images to illustrate the mineralogy and textures of the five styles.

During PMC alteration, the first phase change is that pyrite replaces pyrrhotite. Pyrite occurs as subhedral grains (Fig. 2F) and more commonly, as anhedral intergrowths with chalcopyrite (Fig. 2L). We have observed pentlandite-pyrite-chalcopyrite assemblages (Fig. 2I) and therefore infer that replacement of pyrrhotite by pyrite proceeds to completion before pentlandite starts to alter to millerite. Millerite is present as aggregates of euhedral to subhedral crystals (Fig. 2L). In the most altered samples, there are no primary pyrrhotite or pentlandite grains remaining at all (Fig. 2O). Chalcopyrite is present throughout, and minor cubanite is present in all assemblages, but becomes a more significant constituent at a few modal percent of the sulfide assemblage in the more altered rocks (Fig. 2O). Magnetite is present in very low (< 2%) abundances and is considered to be part of the sulfide assemblage as it commonly occurs as part of fractionated sulfide liquid droplets but not as a constituent of the GNPA host rock (equivalent to the Critical Zone in the rest of the Bushveld Complex, which contains no cumulus magnetite; Eales and Cawthorn, 1996).

The PGM were not systematically characterised in this study as they are described in detail in Smith et al. (2014). Furthermore, due to the resolution of the Mineralogic analysis optimal for the sulfide analysis (5 μm), it was not possible to perform a full PGM study as well as many PGM are smaller than this. However, from Smith et al. (2014), the following relationships can be summarised about the PGM assemblages:

- Style 1 ('primary'): dominated by sperrylite ($PtAs_2$) and the Pd-bismuthotelluride, michenerite (PdBiTe)
- Styles 2–5 ('secondary'): reduction in sperrylite and Pd-bismuthotelluride, with increases in Pd-antimonides (e.g. stibiopalladinite; Pd_5Sb_2), Pt-Pd-tellurides (e.g. telluropalladinite; Pd_9Te_4), electrum (Au-Ag alloy) and a wider range of minerals, including temagamite (Pd_3HgTe_3),

The 'primary' assemblage was interpreted by Smith et al. (2014) to be magmatic, with the more exotic PGM assemblages of the 'secondary' assemblages attributed to fluid alteration causing recrystallization of PGM, but without significant mobilisation of PGE.

6. Quantitative mineral analysis and element deportment

Mineral mapping using Mineralogic Mining software (henceforth referred to as Mineralogic) produced mineral phase maps that quantify both the area and weight percentages of different phases, and also the elemental deportment within each mineral phase (Fig. 1). Fig. 2A,D,G,J and M show example backscattered SEM images of typical thin sections from each style. The Mineralogic phase maps for the same areas are shown in Fig. 2B,E,H,K and N. Quantitative data from the scans of nine sections, which include analysis and identification of over 488,000 individual sulfide and oxide grains, are included in Tables 1 and 2, and Figs. 3–6 show summary data for each stage based on this dataset.

6.1. Relative proportions of minerals in the assemblages

Within the sulfide assemblage, the total area of each sulfide phase was converted to weight percentages by Mineralogic and the relative proportions of each sulfide phase in each mineralisation style are shown in Fig. 3 and Table 1. The minor magnetite may be primary; having crystallised from the initial sulfide liquid, or from oxygen diffusion from sulfide to silicate, and so is included in the dataset. In addition it is considered because magnetite is known to form from the oxidation of sulfide assemblages in some alteration scenarios (e.g. Prichard et al., 2013) and so the Fe in magnetite is considered as part of the Fe budget of the sulfide assembalge.

Style 1 can be considered the 'primary' magmatic sulfide style, composed dominantly of pyrrhotite, with close to equal proportions of pentlandite and chalcopyrite and very minor (< 1 wt%) cubanite and magnetite. Style 2 sees a halving of the proportion of pyrrhotite in the assemblage, and the introduction of a small amount of pyrite. The reduction in the volume, and more ragged texture of pyrrhotite, indicative of replacement by silicates, is evident by comparison of the Mineralogic phase maps in Fig. 2B and E. In terms of the overall proportion of the sulfide assemblage, chalcopyrite and pentlandite increase significantly, but this is relative to the other phases, and does not reflect an actual increase in the abundance of these minerals, but rather a loss of pyrrhotite. Pyrite becomes the most dominant sulfide in Style 3 as pyrrhotite is completely replaced. Chalcopyrite (+cubanite) and pyrite are often intergrown (Fig. 2H, L). The relative proportions of chalcopyrite and pentlandite change through Styles 1–3, with chalcopyrite gradually reducing relative to pentlandite. Millerite is introduced in Style 4 with a corresponding decrease in the proportion of pentlandite, which is completely absent in Style 5.

Magnetite and cubanite are minor constituents of the assemblage throughout. The proportion of magnetite as a percentage of the overall assemblage is very low (< 1% through Styles 1–4), and increases slightly to 1.9% in Style 5. This shows magnetite to be a relatively insignificant constituent of the alteration assemblage, and that alteration of sulfides in this case does not produce magnetite, as serpentinisation commonly does (c.f. Coleman and Keith, 1971). The proportion of cubanite increases at Style 3 to proportions greater than 1% and is at its highest in Style 5, where it comprises 2.4% of the assemblage. Texturally, the sulfides become less disseminated and blebbier as PMC alteration progresses (Fig. 2), perhaps as a result of surface area to volume ratios resulting in preservation of only the largest original blebs.

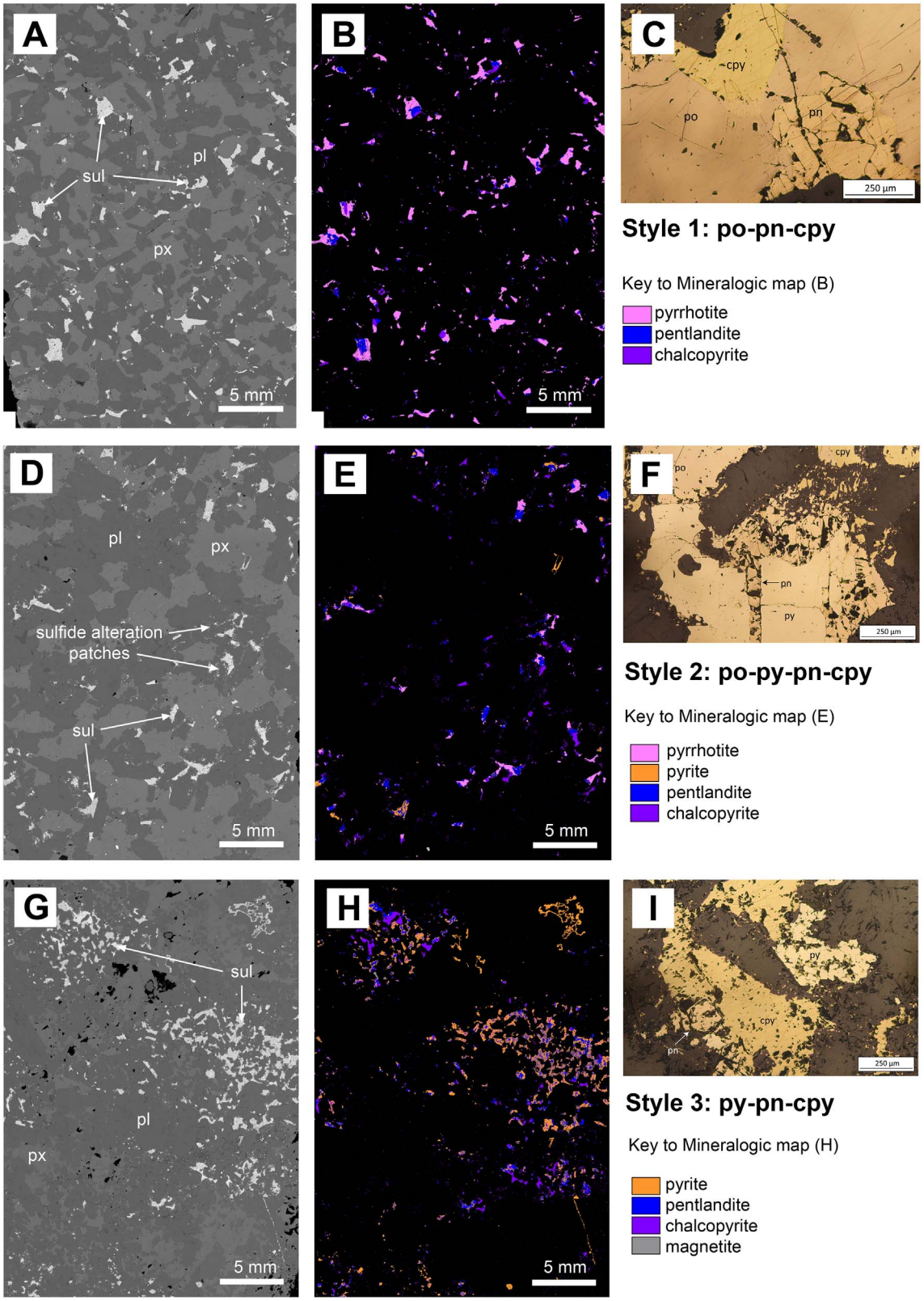

Fig. 2. Sulfide assemblages split into Styles 1–5: A,D,G,J,M: backscattered electron images of thin sections displaying Styles 1–5, respectively; B,E,H,K,N: Mineralogic phase maps of the sulfide-magnetite portions of the sections shown in F-J, respectively; C,F,I,L,O: representative reflected light images of Styles 1–5, respectively. Abbreviations: po = pyrrhotite, pn = pentlandite, cpy = chalcopyrite, py = pyrite, mil = millerite, cub = cubanite, mt = magnetite.

6.2. Major element tenors and ratios of the sulfide assemblage

Fig. 4 shows the proportions of Fe, Ni, Cu and S in the sulfide assemblage as a wt% proportion of the whole sulfide assemblage. Style 1 is dominated by Fe and S reflective of the high proportion of pyrrhotite (Figs. 2B, 3A). At this stage the base metal tenor of the assemblage is around 5 wt% Cu and 4 wt% Ni. There is a major drop in Fe in Style 2 (with removal of pyrrhotite), which approximately doubles the Cu and

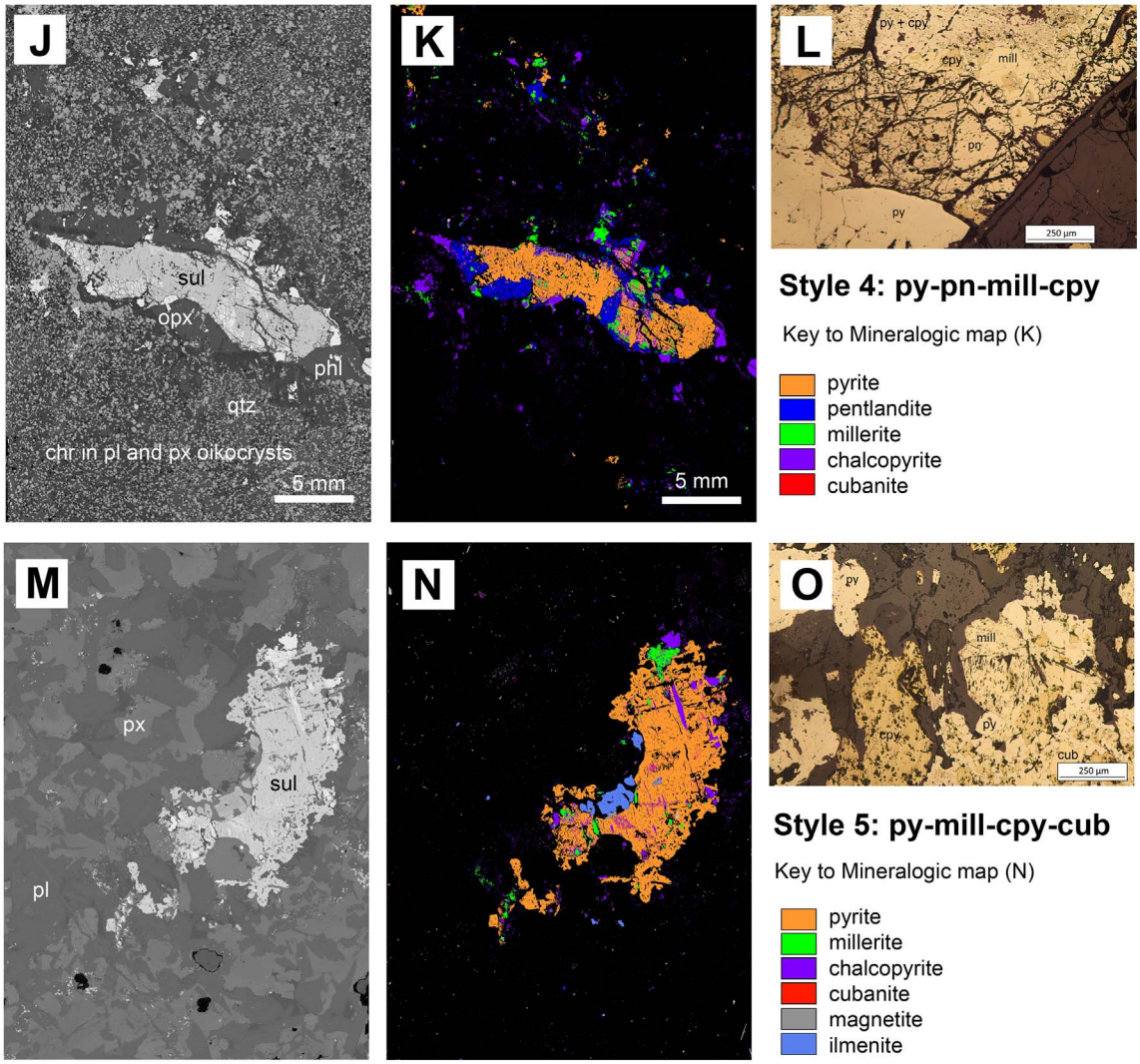

Fig. 2. (*continued*)

Ni tenors. The overall Fe-Cu-Ni-S composition of the assemblage remains fairly consistent through Styles 2–4, with only minor relative decreases in Fe at each stage. This implies that the mineralogical changes occurring during these stages, primarily pentlandite to millerite (+pyrite), do not significantly affect the overall metal ratios (but may still involve mass loss that is consistent across all elements). The Cu and Ni tenors are similar throughout Styles 2–3 but in Style 4, and especially the transition to Style 5, see a reduction in the Cu tenor relative to Ni, consistent with the respective decrease in chalcopyrite relative to millerite (Fig. 3D,E).

It should be noted that the data shown in Fig. 4 are proportional and normalised to the bulk sulfide assemblage and not scaled to reflect any relative volume at each stage. Thus, the relative increases in Ni and Cu from Style 1 to Style 2, for example, are not reflective of the addition of those elements, but more of the preferential removal of Fe and S during that stage. To illustrate this, a number of ratios are shown in Fig. 5A. There are some clear trends that track across the continuum of stages. The Ni/Fe ratio increases through Styles 1–4, consistent with progressive Fe-loss during those stages. The Fe/S ratio decreases consistently throughout the same stages, again consistent with progressive Fe-loss. The Ni/S ratio, however, increases over Styles 1–4, and Cu/S increases strongly from Style 1 to 2, meaning that S is being lost relative to Ni and Cu in these early stages. As such, the PMC alteration tracks early S-loss, alongside even more pronounced Fe-loss. The Ni/Cu ratio increases at each stage, and indicates Cu loss relative to Ni throughout PMC alteration, but especially in the final stage where the ratio increases by the greatest amount to a maximum of 2.95. A number of the ratios reverse in Style 5, with Cu/Fe and Cu/S reducing, suggestive of pronounced Cu loss in the final stage, and perhaps some S addition. A reduction in Ni/Fe and Ni/S in Style 5 would reflect minor Ni loss, or S addition.

As Ni is the least mobile of the four major elements (Liu et al., 2012), the Cu, Fe and S contents have been normalised to Ni in Fig. 5B to show the behaviour of these elements assuming that no Ni is lost or added during the alteration process (an assumption tested later). This highlights the loss of both S, and to a greater extent, Fe, in the earliest styles of PMC alteration (Style 1 to 2). Clearly, the early removal of pyrrhotite has a significant effect on the S and Fe content of the sulfide within the rock, with a loss of over half of the bulk S and over two thirds of the bulk Fe, relative to Ni (Fig. 5B), as seen by the doubling of Ni and Cu tenor (Fig. 4B). Copper is seen to gradually decrease compared to Ni (from Cu/Ni 1.1 to 0.3 over the five styles), but is more prominently lost in the final two styles (also seen in sharp increase in Ni/Cu ratio on Fig. 5A). Interestingly, the S/Ni and Fe/Ni ratios both increase from Style 4 to 5. This would be consistent with either some Ni loss (though proportionally less than the Cu loss), or the addition of Fe-sulfide. If the latter is correct, this would be the only addition of mass in a process of alteration that progressively reduces the mass of the sulfide (also tested below).

Table 1
Bulk sample data from representative thin sections calculated by Mineralogic Mining. 'Number' is the number of individually identified grains at the resolution scanned (5 μm), and 'grain size' refers to the mean diameter of all grains of that phase.

	Number	Area %	Wt %	Grain Size (μm)	Grain Size Std Dev (μm)	Proportion by wt%
RP04-23 338	Style 1					
Pyrrhotite	3165	76.28	78.33	31.99	93.59	78.35
Pentlandite	1786	9.29	9.93	21.89	45.73	9.93
Chalcopyrite	5032	12.18	11.37	17.79	29.36	11.37
Cubanite	1277	0.28	0.25	5.94	3.1	0.25
Magnetite	257	0.08	0.09	7.66	4.76	0.09
RP04-23 374	Style 1					
Pyrrhotite	2481	67.83	69.43	63.46	107.07	69.44
Pentlandite	2334	13.57	14.47	27.45	50.19	14.47
Chalcopyrite	7301	16.54	15.39	18.55	30.79	15.39
Cubanite	2033	0.44	0.39	6.78	4.48	0.39
Magnetite	159	0.28	0.32	21.85	31.87	0.32
RP05-37 69	Style 2					
Pyrrhotite	2189	27.2	27.95	41.61	81.91	27.96
Pyrite	2636	9.33	10.42	24.57	47.86	10.43
Pentlandite	7341	29.2	31.24	26.22	44.67	31.25
Chalcopyrite	20637	30.17	28.18	16.05	27	28.2
Cubanite	2267	0.39	0.35	6.52	3.85	0.35
Magnetite	2774	1.58	1.81	12.86	11.53	1.81
ORL4	Style 2					
Pyrrhotite	9683	44.2	45.83	63.51	130.73	45.86
Pyrite	22444	3.71	4.18	9.67	26.35	4.18
Pentlandite	34491	28.26	30.51	28.27	57.85	30.53
Chalcopyrite	41847	20.4	19.22	20.41	43.88	19.23
Cubanite	8896	0.25	0.22	6.47	5.68	0.23
Magnetite	275	0.01	0.01	6.85	5.64	0.01
RP04-21 681	Style 3					
Pyrite	6716	48.63	53.08	46.93	77.54	54.19
Pentlandite	15685	23.58	24.66	19.78	34.78	25.17
Chalcopyrite	22457	20.24	18.47	14.6	25.47	18.86
Cubanite	13398	1.97	1.73	7.64	5.46	1.77
Magnetite	18	0.01	0.01	11.47	8.04	0.01
RP04-23 158	Style 3					
Chalcopyrite	14119	12.26	11.12	12.82	21.05	17.81
Cubanite	5776	0.91	0.8	6.43	3.86	1.27
Magnetite	157	0.06	0.06	9.49	8.9	0.1
Pentlandite	9863	14.09	14.65	17.26	27.04	23.46
Pyrite	4170	33.02	35.83	37.68	68.76	57.36
RP05-45 167B	Style 4					
Pyrite	5898	46.73	49.24	41.72	110.68	49.36
Pentlandite	19882	18.13	18.3	24.68	32.33	18.35
Millerite	2299	8.65	10	47.9	74.86	10.03
Chalcopyrite	38131	24.01	21.16	16.71	31.58	21.21
Cubanite	17268	1.19	1.01	7.25	6.17	1.01
Magnetite	952	0.04	0.05	5.4	2.37	0.05
RP05-45 205B	Style 5					
Pyrite	6517	52.55	53.18	47.34	124.37	53.39
Millerite	2906	27.65	30.72	63.92	124.89	30.84
Chalcopyrite	21807	13.36	11.31	18.16	31.98	11.35
Cubanite	40080	4.73	3.85	11.08	12.25	3.87
Magnetite	1722	0.53	0.55	14.73	17.91	0.55
RP05-45 165	Style 5					
Pyrite	2946	68.59	73.18	95.90	194.71	73.47
Millerite	864	3.72	4.36	48.01	89.47	4.38
Chalcopyrite	22412	9.73	8.69	15.07	28.98	8.72
Cubanite	20413	1.07	0.92	6.97	4.40	0.92
Magnetite	10490	2.59	2.84	13.70	18.59	2.85

6.3. Elemental deportment of the sulfides

The elemental deportment of Fe, Ni, Cu and S as determined by Mineralogic (Table 2 – distributions) is shown in Fig. 6. The majority of the S is present in pyrrhotite in Style 1 (Fig. 6A), which, as shown above, is lost very quickly, meaning the deportment of S in the remaining sulfide quickly changes to being dominantly held by pyrite from Style 3 onwards. The deportment of Fe is very similar to that of S (Fig. 6B), which reflects its dominant Fe-sulfide host, either as pyrrhotite or pyrite. The proportion of Fe that is present in magnetite is very small but is highest (3.2%) in the final alteration style. The deportment of Ni is controlled by pentlandite, and the transition to millerite is clearly shown in Stage 4, with a trace amount of Ni also held in some pyrite in the latter styles. Copper is present as chalcopyrite in all assemblages, with a slight increase in the proportion held by cubanite in Style 5.

6.4. Trace element tenors of the sulfide assemblage

The average concentrations of a number of trace elements in pyrrhotite, pentlandite, pyrite, millerite, chalcopyrite and cubanite, as determined by LA-ICP-MS (data from Smith, 2014; Table A1), were used to calculate the tenors of the overall sulfide assemblage at each stage (Table 3), using the mineral proportions shown in Fig. 2 and Table 1. These elements were chosen as they occur largely or exclusively in solid solution in the sulfide phases and thus the LA-determined concentrations represent the concentration in the sulfide as a whole with fidelity (Smith et al., 2014). Cobalt has not been included in the datset we present here as it is highly variable in the original dataset from Smith (2014) due to zonation across crystals, particularly pyrite, and thus the individual LA analyses are not accurately representative of the tenors of the sulfides as a whole.

Elements such as Pt, Te and Au are commonly present as discrete minerals (e.g. Pt-tellurides, electrum) and concentrations determined by LA-ICP-MS of sulfides are strongly controlled by the presence or absence of these phases (as 'micro-nuggets') in the volume of sulfide ablated. Whilst some Pt, Au and Te may be present in solid solution in pyrite, we do not include these elements here as the heterogeneous distribution means that the LA data are not representative of the tenors in sulfide, and no significant Pt is present in the Style 1 sulfides (i.e. it is almost exclusively present as PGM). Samples from the dataset by Smith (2014) were re-examined and classified as Styles 1–5. The mean value for each trace element in each sulfide phase from each style was determined. Due to the variability between individual LA-ICP-MS analysis, the trace element data presented here can be considered to be semi-quantitative.

As established above, there is compelling evidence for a mass loss of sulfide during the PMC alteration. Most trace elements held in sulfide, show increases in tenor as alteration progresses, with the most consistent being Bi and Rh, which increase by more than an order of magnitude (Fig. 7). Rhodium shows an increase from 0.2 ppm in Style 1 to 4.1 ppm in Style 5, and Bi increases from 1.3 ppm to 31 ppm (Table 3). Selenium also increases overall, but is more erratic, and actually peaks at Style 3.The IPGE (Os, Ir, Ru) all show similar trends to one another, as would be expected due to their very similar behaviour, with a prominent dip at Style 3 but an increase in tenor overall of just less than an order of magnitude. It is difficult to envisage that the Rh and IPGE are added in the final stage due to their immobility in most hydrothermal conditions, and thus the increase in tenor in Stage 5 reflects further mass loss of sulfide. As such, this would mean that the patterns shown in Fig. 5B confirm Ni loss in the final stage, and not S gain.

The most striking trend shown is that of Pd, which increases in tenor steadily from 1.6 ppm in Style 1, to 40 ppm in Style 4 assemblages (Table 3). However, it drops off dramatically in Style 5 to only 3.4 ppm (Fig. 7; Table 3). This indicates a significant Pd loss from the sulfide in the transition to Style 5, which is decoupled from the IPGE, Rh, Se and Bi, which all show an increase in tenor in Style 5. Thus, the final stage of alteration that produces the Style 5 assemblage sees an increase in tenor of most trace elements, but a significant loss of Pd, alongside losses of Cu and some Ni.

Table 2
Assay data determined by Mineralogic for the sulfide-magnetite assemblage for representative thin sections. Distribution data used for deportment shown in Fig. 6.

	Mineral wt %	Assay(S)%	Distrib (S)%	Assay (Fe)%	Distrib (Fe)%	Assay (Ni)%	Distrib (Ni)%	Assay (Cu)%	Distrib (Cu)%
RP04-23 374	STYLE 1								
Chalcopyrite	15.39	4.89	13.76	5.03	9.37	0	0.1	5.35	98.34
Cubanite	0.39	0.12	0.34	0.15	0.27	0.03	0.61	0.08	1.45
Magnetite	0.32	0	0	0.31	0.58	0	0	0	0
Pentlandite	14.47	4.45	12.53	4.92	9.18	5.07	98.8	0	0
Pyrrhotite	69.43	26.08	73.36	43.26	80.6	0.02	0.49	0.01	0.21
Assemblage		35.54		53.67		5.13		5.44	
RP04-23 338	STYLE 1								
Chalcopyrite	11.37	3.79	10.12	3.61	6.59	0	0.05	3.79	98.59
Cubanite	0.25	0.07	0.2	0.09	0.16	0.01	0.43	0.05	1.3
Magnetite	0.09	0	0	0.06	0.12		0	0	0
Pentlandite	9.93	3.21	8.58	3.26	5.95	3.38	99.28	0	0
Pyrrhotite	78.33	30.37	81.1	47.79	87.18	0.01	0.24	0	0.11
Assemblage		37.45		54.81		3.4		3.84	
RP05-37 69	STYLE 2								
Chalcopyrite	28.18	9.4	26.17	8.89	20.85	0	0.03	9.53	99.25
Cubanite	0.35	0.13	0.36	0.13	0.3	0.02	0.15	0.06	0.65
Magnetite	1.81	0.01	0.02	1.8	4.22	0	0	0	0
Pentlandite	31.24	9.96	27.73	10	23.47	11.23	99.01	0	0
Pyrite	10.42	5.49	15.28	4.83	11.32	0.08	0.72	0.01	0.07
Pyrrhotite	27.95	10.94	30.45	16.98	39.83	0.01	0.09	0	0.03
Assemblage		35.92		42.63		11.34		9.6	
ORL 4	STYLE 2								
Chalcopyrite	19.22	6.52	17.71	6.05	13.35	0	0.02	6.4	99.29
Cubanite	0.22	0.08	0.22	0.08	0.18	0.01	0.08	0.04	0.65
Magnetite	0.01	0	0	0.01	0.01	0	0	0	0
Pentlandite	30.51	9.82	26.67	9.65	21.31	10.75	99.79	0	0
Pyrite	4.18	2.15	5.86	1.94	4.28	0	0.04	0	0.04
Pyrrhotite	45.83	18.23	49.54	27.55	60.87	0.01	0.07	0	0.02
Assemblage		36.8		45.27		10.77		6.45	
RP04-21 681	STYLE 3								
Chalcopyrite	18.47	6.14	14.44	5.83	15.16	0	0.03	6.18	94.75
Cubanite	1.73	0.7	1.65	0.67	1.74	0.02	0.2	0.3	4.53
Magnetite	0.01	0	0	0.01	0.03	0	0	0	0
Pentlandite	24.66	7.8	18.34	7.39	19.22	9.19	94.85	0	0
Pyrite	53.08	27.88	65.58	24.54	63.85	0.48	4.92	0.05	0.72
Assemblage		42.52		38.44		9.69		6.52	
RP04-23 158	STYLE 3								
Chalcopyrite	11.12	3.74	13.47	3.49	14.21	0	0.04	3.66	95.93
Cubanite	0.8	0.28	1	0.3	1.21	0.01	0.17	0.14	3.71
Magnetite	0.06	0	0	0.05	0.19		0	0	0
Pentlandite	14.65	4.66	16.81	4.31	17.55	5.41	99.59	0	0
Pyrite	35.83	19.06	68.72	16.44	66.85	0.01	0.2	0.01	0.35
Assemblage		27.74		24.59		5.43		3.81	
RP05-45 167B	STYLE 4								
Chalcopyrite	21.16	6.95	16.44	6.78	19.08	0.02	0.11	7.29	97.18
Cubanite	1.01	0.43	1.03	0.4	1.13	0	0.03	0.16	2.19
Magnetite	0.05	0	0.01	0.04	0.12	0	0	0	0
Millerite	10	3.39	8.03	0.11	0.3	6.49	45.53	0	0
Pentlandite	18.3	5.71	13.51	4.9	13.8	7.67	53.78	0	0.01
Pyrite	49.24	25.78	60.98	23.3	65.56	0.08	0.55	0.05	0.62
Assemblage		42.27		35.53		14.26		7.5	
RP05-45 205B	STYLE 5								
Chalcopyrite	11.31	3.7	8.56	3.68	11.84	0.06	0.28	3.85	83.67
Cubanite	3.85	1.67	3.86	1.57	5.04	0	0.02	0.61	13.24
Magnetite	0.55	0	0	0.54	1.75	0	0	0	0
Millerite	30.72	10.23	23.69	0.17	0.53	20.3	98.52	0	0.01
Pyrite	53.18	27.6	63.89	25.14	80.83	0.24	1.18	0.14	3.08
Assemblage		43.2		31.1		20.6		4.6	
RP05-45 165	STYLE 5								
Chalcopyrite	8.69	2.86	6.64	2.77	7.03	0.01	0.22	2.93	94.16
Cubanite	0.92	0.37	0.85	0.36	0.92	0	0.01	0.15	4.93
Magnetite	2.84	0	0	2.14	5.44	0	0	0	0
Millerite	4.36	1.46	3.39	0.02	0.05	2.79	94.76	0	0
Pyrite	73.18	38.46	89.12	34.05	86.57	0.15	5.01	0.03	0.9
Assemblage		43.15		39.33		2.94		3.11	

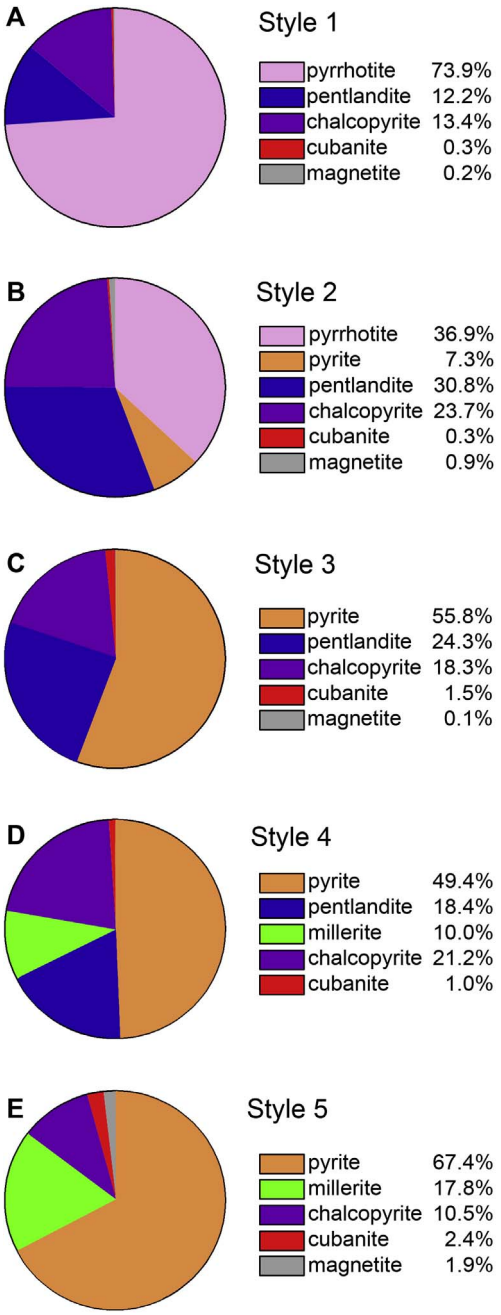

Fig. 3. Pie charts showing the wt% proportions of each mineral in the sulfide-magnetite assemblages from Styles 1–5 (A-E, respectively). Data from Table 1.

6.5. Trace element deportment

To further understand some of the relationships shown in Fig. 7, we illustrate the mineralogical deportment of each trace element through the alteration stages in Fig. 8 (and Table A2). This takes into account the relative proportions of each sulfide mineral (Fig. 2 and Table 1), and the mean concentrations from the LA data (Table A1), and essentially shows the mineralogical split for each data point in Fig. 7.

Palladium is hosted largely by pentlandite (Fig. 8A), and minor pyrite, and the increase in Pd tenor of the sulfide assemblage as a whole shown in Fig. 7 reflects an increasing tenor in the pentlandite through Styles 1–4. Our data show that millerite does not hold any significant Pd in solid solution and thus the increase in Pd tenor of the pentlandite is likely linked to the reduction in volume of pentlandite, but with Pd restricted to the pentlandite that remains, or at least recrystallizing with

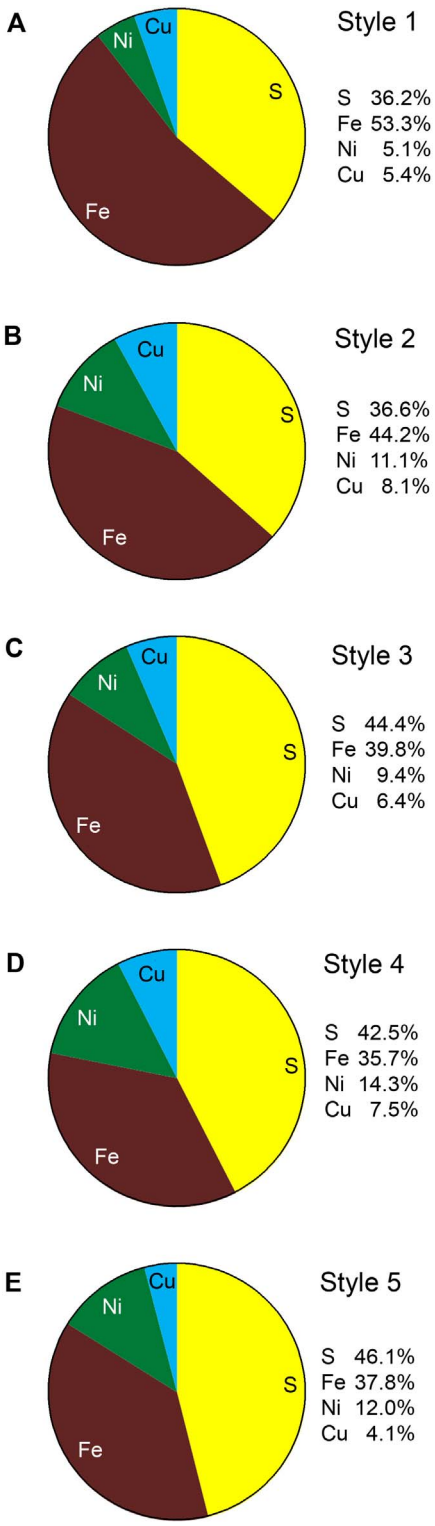

Fig. 4. Pie charts showing the wt% proportions of S, Fe, Ni and Cu in the sulfide-magnetite assemblages from Styles 1–5 (A-E, respectively). Data from Table 2.

it as the volume of pentlandite decreases. The disappearance of pentlandite in Style 5 explains the sharp drop in bulk sulfide Pd tenor (Fig. 7). This can only be explained by Pd loss from the sulfide, and more specifically, pentlandite. As such, this shows that during PMC alteration, Pd is effectively held within pentlandite, to higher concentrations with decreasing volumes of pentlandite, until being liberated when pentlandite is fully lost, and that it is not taken up in any significant amounts by the alteration product of pentlandite, millerite,

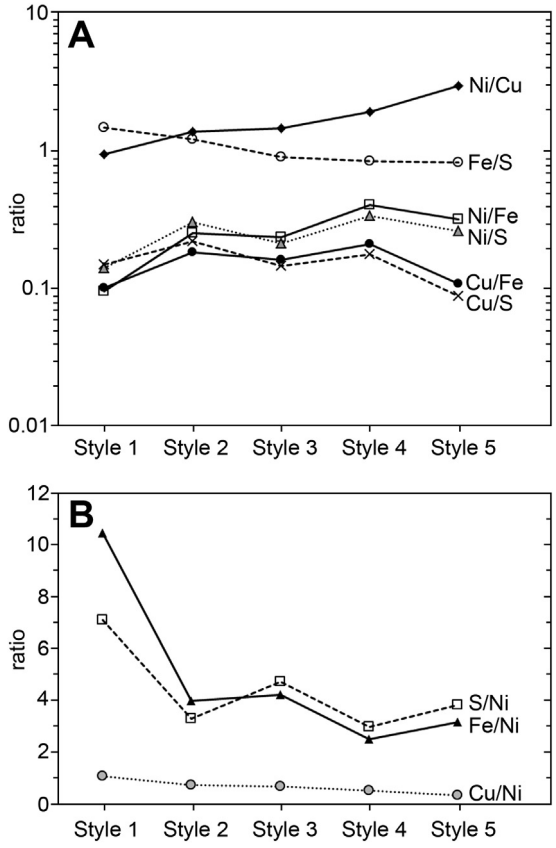

Fig. 5. A: inter-element ratios of S, Fe, Ni and Cu through each style of alteration; B: ratios of S, Fe and Cu to Ni through each style of alteration.

though minor amounts are present in secondary pyrite.

In contrast to Pd, Rh and the IPGE appear to be effectively transferred from their primary hosts (pyrrhotite and pentlandite) into secondary pyrite (Fig. 8B-E). The dip in bulk IPGE tenor at Style 3 (Fig. 7) corresponds with loss of pyrrhotite (Fig. 8B-D), which is known to be a significant host of IPGE in magmatic sulfide deposits (Holwell and McDonald, 2007, 2010; Godel et al., 2007; Osbahr et al., 2013; Duran et al., 2016; Klemd et al., 2016), but this may indicate that they are not transferred in full to the pyrite that replaces pyrrhotite. This has been suggested by Duran et al. (2015) for pyrite in the Lac des Iles complex, though was not quantitatively assessed. The IPGE are also hosted by pentlandite and the bulk tenor increases through Styles 3–5 (Fig. 7), with much of this being held in pyrite (Fig. 8B-D). This indicates that the IPGE are transferred effectively from pentlandite to pyrite and not to millerite during the latter stages of alteration. Interestingly, Rh is not significantly hosted by pentlandite (Fig. 8E) as it has shown to be in many magmatic sulfide assemblages (Holwell and McDonald, 2010). It is overwhelmingly controlled by pyrite, and appears to partition in pyrite as soon as it appears, in Style 2. The highest tenors of Rh (4 ppm; Fig. 8E) in the Style 5 pyrite attest to no significant Rh loss during the alteration process.

The two semi metals that are present largely in solid solution (Se and Bi) have very different behaviours as alteration progresses. Fig. 7 shows Se tenor increases overall, though there is a spike at Style 3, and Bi also shows an overall, though much sharper increase through the continuum of styles (Fig. 7). However, the mineralogical deportment of the two semi metals contrasts significantly. Selenium deportment largely reflects the overall sulfide assemblage (c.f. Fig. 8F and Fig. 3) and shows that Se is present in all sulfide phases. The overall general increase in Se tenor also supports net S loss, with Se preferentially accommodated in the sulfide that remains. This would reduce bulk rock S/Se ratios with alteration, which Smith et al. (2016) demonstrated to be true for altered GNPA rocks. In contrast, Bi shows very similar behaviour to Rh, being taken up preferentially by pyrite as soon as it appears in the assemblage. Fig. 8G also shows that Bi held in pentlandite in the early stages is effectively taken up by millerite in the latter stages.

7. Alteration assemblages

Alteration within the GNPA is highly variable, and is mostly restricted to the sulfides, with Smith et al. (2011) illustrating some remarkably fresh plagioclase-two-pyroxene-(chromite) cumulates, and others with sericitisation of plagioclase and minor amphibole

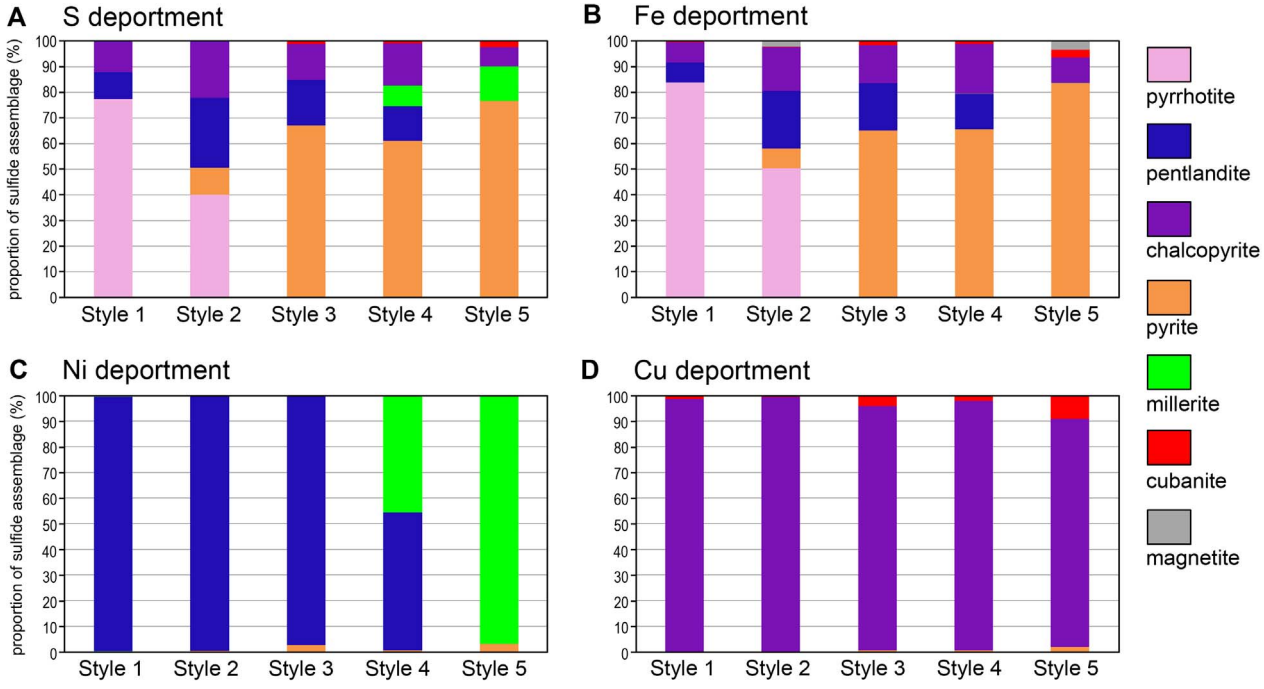

Fig. 6. Mineralogical deportment of A: S; B: Fe; C: Ni and D: Cu in each style (data from Table 2).

Table 3
Tenors of trace elements found in solid solution in bulk sulfide calculated from the proportions of different sulfide phases (means from each stage in Table 1, and LA-ICP-MS data from Smith et al. (2014); Table A1), shown in Fig. 7. Break down of tenors of individual sulfide phases in each stage are shown in Table A2 and Fig. 8.

	Os (ppm)	Ir (ppm)	Ru (ppm)	Rh (ppm)	Pd (ppm)	Bi (ppm)	Se (ppm)
Style 1	0.26	0.21	1.74	0.2	1.64	1.28	113.68
Style 2	0.39	0.34	2.68	0.75	10.62	4.43	116.63
Style 3	0.16	0.11	0.47	2.41	20.93	16.14	197.15
Style 4	0.24	0.4	1.75	1.89	40.43	12.68	132.79
Style 5	1.5	1.16	12.14	4.07	3.37	31.04	149.09

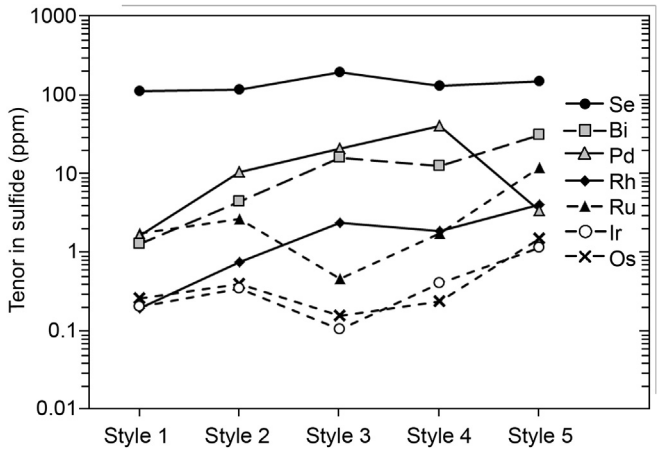

Fig. 7. Trace element tenors in sulfide through each style of alteration (data from Table 3).

replacement of pyroxenes. Table 1 of Smith et al. (2011) records the amount of silicate alteration in a suite of 37 samples. From this, there is no consistent correlation between the amount of alteration with stratigraphic height, with it being present throughout the ~400 m sequence. However, alteration appears to be more common where the floor rocks is comprised of metasedimentary rocks. In comparison, in holes where Lower zone cumulates make up the floor rocks to the GNPA, alteration is less common in the overlying GNPA basal unit. Nevertheless, Smith et al. (2011) concluded that the alteration present in the GNPA member was linked with the alteration of the sulfides on textural grounds. The source of the fluids may be related to wall-rock interaction during emplacement, given the higher proportions of alteration where the GNPA Member is in contact with the floor rocks, though the upper parts of the GNPA Member display sulfide alteration irrespective of footwall type.

The quantitative evidence from the ore mineralogy clearly shows mass loss from the sulfide assemblage. As such, the altered sulfides should show evidence of a volume reduction with a corresponding increase in alteration minerals. Fig. 9 illustrates a number of textures in the GNPA rocks where sulfides from Styles 2–5 (pyrite-bearing) are surrounded by quartz, chlorite, hydrous silicates such as phlogopite and very minor actinolite, altered (sericitised) plagioclase and some orthopyroxene. Smith et al. (2011) illustrated some of these (e.g. Fig. 9B,C), and noted they were associated with the sulfides, and stated that the chromite-poor zones surrounding sulfide blebs in the chromitites (e.g. Fig. 9C,D) may represent small pockets of trapped silicate liquid containing sulphide droplets. This may explain the presence of orthopyroxene and altered plagioclase in the zones around the replaced sulfides if they formed from a silicate melt. Alternatively, the quartz-phlogopite-chlorite-bearing zone around the sulfide in Fig. 9C and D may represents the original area filled with sulfide and bounded by coarse chromite. The alteration then reduced the volume of the sulfide, moving the grain boundary inwards and precipitating silicate minerals in its place, with chromite that marked the original boundary remaining unaltered (Fig. 9). It may be that the silicate pockets represent both of these possibilities, with some of the silicates being the product of trapped pockets of volatile-rich silicate melt (with associated sulfide droplets), which have subsequently been partially replaced by hydrous silicates. If so, then the boundaries inferred in Fig. 9 represent maximum volume losses, and would be large overestimates.

However, as an end member assessment of the volume loss, if we interpret the textures to represent purely alteration assemblages, image analysis of the reduction in sulfide *area* shown by the sections in Fig. 9A-D is 36% (Style 2), 46% (Style 3), 50% (Style 4) and 75% (Style 5), respectively. For a qualitative indication of the volume loss, we can assume that the sections shown in Fig. 9 represent a central section through two ellipses (analogous to a section through the centre of a hard-boiled egg). Using the long and perpendicular axes of idealised ellipses around the sulfide and the alteration area, the *volume* reduction in Fig. 9A-D is equivalent to 35% (Style 2), 60% (Style 3), 58% (Style 4), and 88% (Style 5), respectively. Thus, this would imply up to an order of magnitude reduction in sulfide volume from the textural data.

8. Mass balance for Fe, Cu, Ni and S

A quantitative mass balance for all elements during PMC alteration is not possible without independent evidence for the chemistry of the fluids, which is not available. Furthermore, the inherent uncertainties in using mean values in the trace element data, and more significantly, their presence as other phases (such as PGM) that we have not quantified does not allow for this without a full PGM quantification, which is out of the scope of this study. However, our quantitative data for the major components of the sulfide assemblage allow us to make a semi-quantitative mass balance for Fe, Cu, Ni and S. The basis for this is illustrated in Fig. 5B, where Fe, Cu and S are normalised to Ni as the least mobile element. However, we have shown that some Ni is certainly lost in at least the final stages of PMC alteration, and as such, we require another independent, immobile parameter to normalise our data to.

From the trace element data shown in Fig. 7, Rh tenors appear to increase through the alteration assemblage. It is almost certainly highly immobile in hydrothermal fluids and is highly unlikely to have been introduced by any hydrous fluids and therefore offers an alternative normalising element instead of Ni. Smith et al. (2014) do report hollingworthite (RhAsS) in the GNPA rocks in both primary and secondary assemblages, so there is a possibility of some recrystalisation of Rh from or to PGM that our mass balance doesn't account for, but we consider Rh to be a much more robust normalising element than Ni. The ratios of Fe, Cu, Ni and S over Rh are plotted in Fig. 10 and the consistent slope in all but the transition from Style 3 to 4 shows that Ni is lost *throughout* PMC alteration relative to Rh. As such, if we assume Rh to be immobile throughout the alteration process, the ratios of Fe, S, Ni and Cu to Rh would indicate that in the transition from Style 1 to 2, a loss of 78% of the Fe, 73% of the S, 63% of the Cu and 42% of the Ni has occurred. The major significance of this is that the first stage of alteration not only removes Fe, S and Cu, but also significant Ni. Using Rh as an immobile normalisation factor indicates a loss of over 90% of the sulfide assemblage in the most altered rocks in Style 5.

Such reductions in volume are consistent with the image analysis of the textures illustrated in Fig. 9, which imply a volume loss of around

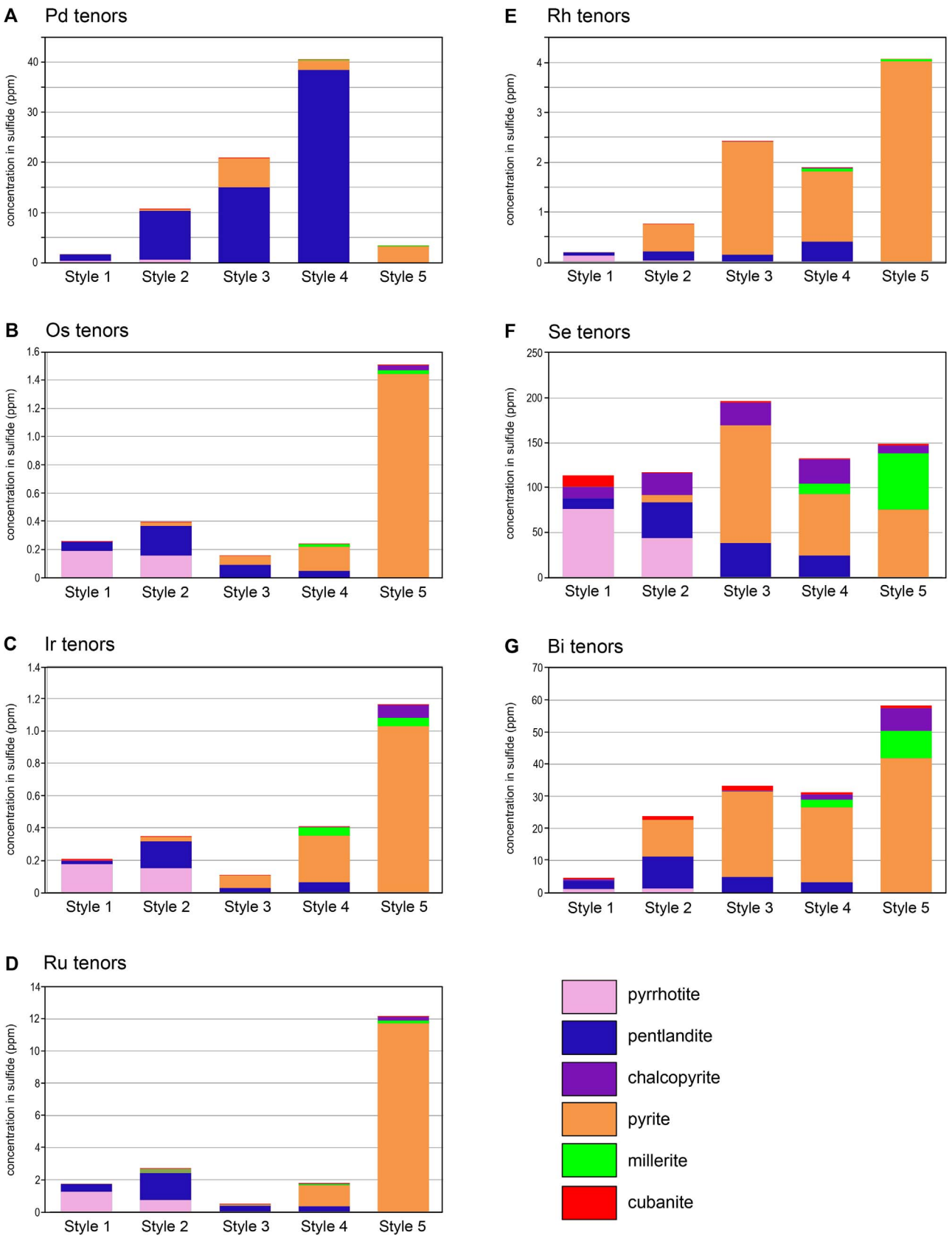

Fig. 8. Mineralogical deportment of trace elements through each style of alteration: A: Pd; B: Os; C: Ir; D: Ru; E: Rh; F: Se; G: Bi.

60% by Styles 3–4 (Fig. 9B-C) and up to 88% in Style 5 (Fig. 9D). Therefore, the use of Rh as an incompatible normalising factor seems to be consistent with the observed textures that indicate up to 90% volume loss of sulfide. As such, the trace element approach is independently verified by the textural evidence and supports significant (an order of magnitude) loss of Cu-Ni-Fe-S and subsequent replacement by silicates,

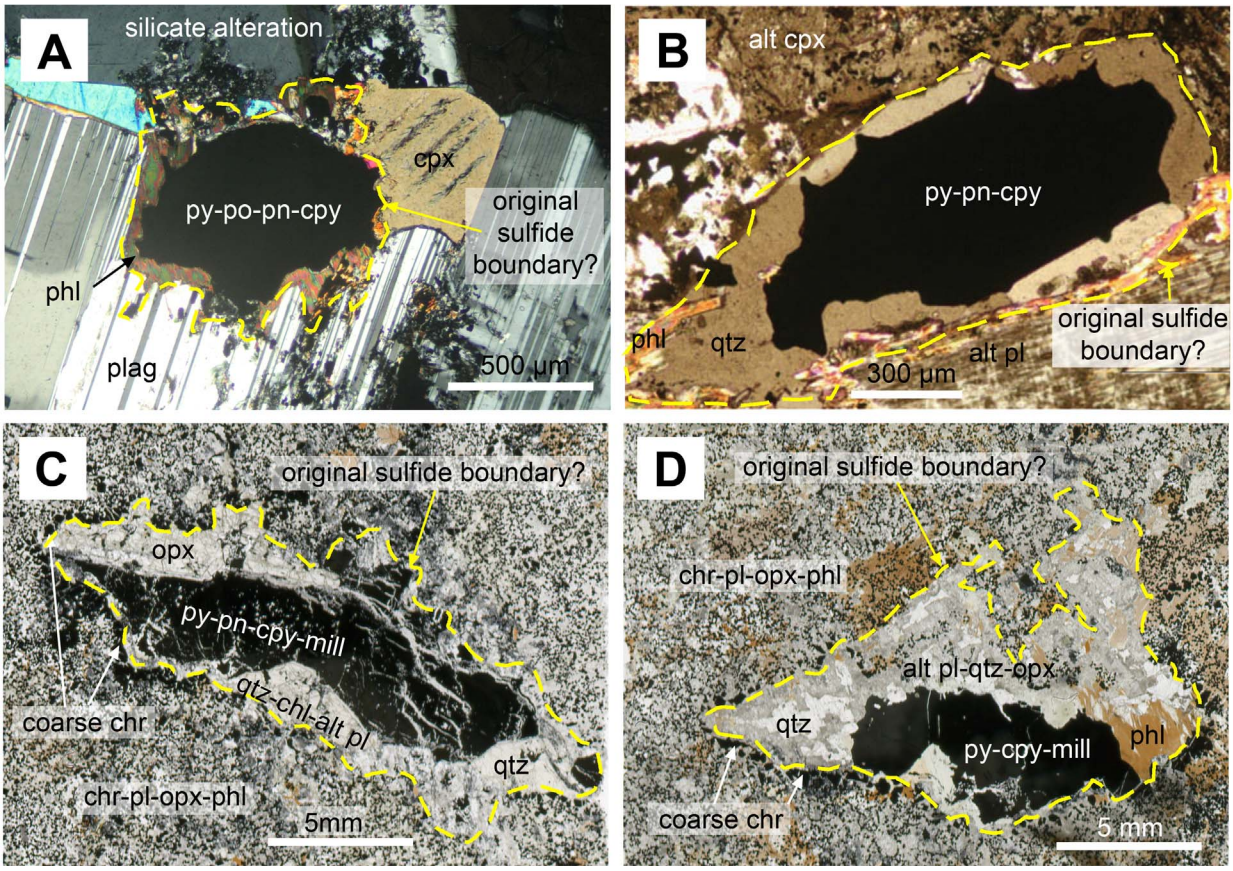

Fig. 9. Silicate alteration assemblages and textures around altered silicates. A: Style 2 sulfide assemblage surrounded by phlogopite alteration with some sericite alteration of plagioclase; B: Style 3 alteration surrounded by quartz and minor phlogopite alteration; C: Style 4 (also shown in Fig. 2J-L) alteration in chromitiferous gabbronorite, with silicate alteration around sulfide by quartz, phlogopite, chlorite and orthopyroxene; D: Style 5 alteration in chromitiferous gabbronorite, with silicate alteration around sulfide by quartz, phlogopite, chlorite, altered plagioclase and orthopyroxene. py = pyrite, po = pyrrhotite, pn = pentlandite, cpy = chalcopyrite, mill = millerite, qtz = quartz, phl = phlogopite, chl = chlorite, alt pl = altered plagioclase, cpx = clinopyroxene, opx = orthopyroxene, chr = chromite.

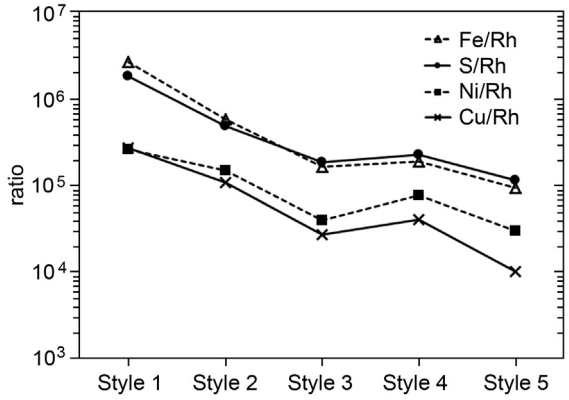

Fig. 10. Ratios of S, Fe, Ni and Cu to Rh through each style of alteration.

which contain some Fe, but little or no Cu, Ni or S. Thus, PMC alteration involves significant mobilisation of Cu, Ni and S.

9. Modelling results

An equilibrium reaction path model titrated an idealised silicate-sulfide composition into a synthetic hydrothermal fluid (heated seawater). Results are expressed in terms of water-rock ratio (Log w/r); increasing w/r reflects increased or continued flux of a hydrothermal fluid through the rock. At very low values of Log w/r (< −1) the water is consumed by the hydration of silicate phases (Reed, 1997). Fig. 11 shows that both the sulfide (Fig. 11A) and the silicate (Fig. 11B) assemblages are modified by hydrothermal alteration. In the range of log w/r values considered (−1 to 1), the total sulfides decreases from 5 wt% in the initial composition to ~4 wt%. This is not as extreme as that suggested by the textural and metal tenor data, but still indicates the process reduces the amount of sulfide in the rock.

The sulfide mineral assemblage evolves from an initial 3 wt% pyrrhotite, 1 wt% pentlandite and 1 wt% chalcopyrite (as a percentage of the total rock). Pyrite increases at the expense of pyrrhotite, until the assemblage is ~2 wt% pyrite, 1 wt% pentlandite and 1 wt% chalcopyrite at log w/r 0.2. By log w/r 0.5 and higher, pentlandite has been replaced by millerite (0.5 wt%), accompanied by 1 wt% chalcopyrite and 2.5 wt% pyrite. The sequence of mineralogical changes run by the model *exactly* replicates that of our observations of the PMC altered GNPA Member rocks, and the equivalent Styles are annotated on Fig. 11. The model confirms that all pyrrhotite is replaced before millerite appears, and thus our recognition of Style 3 as pyrite-pentlandite-chalcopyrite is corroborated thermodynamically. The modelled silicate assemblage (Fig. 11B) is approximately 45 wt% pumpellyite, 25 wt% chlorite, 12 wt% diopside (clinopyroxene), 10 wt% quartz, and minor hedenbergite (orthopyroxene). The consistency between the modelling and the observed mineralogy is discussed below.

10. Discussion

The low temperature hydrothermal alteration of magmatic pyrrhotite-pentlandite-chalcopyrite assemblages to pyrite-millerite-chalcopyrite involves a progressive change in mineralogy and element deportment, alongside a significant mass loss. Whilst this has been

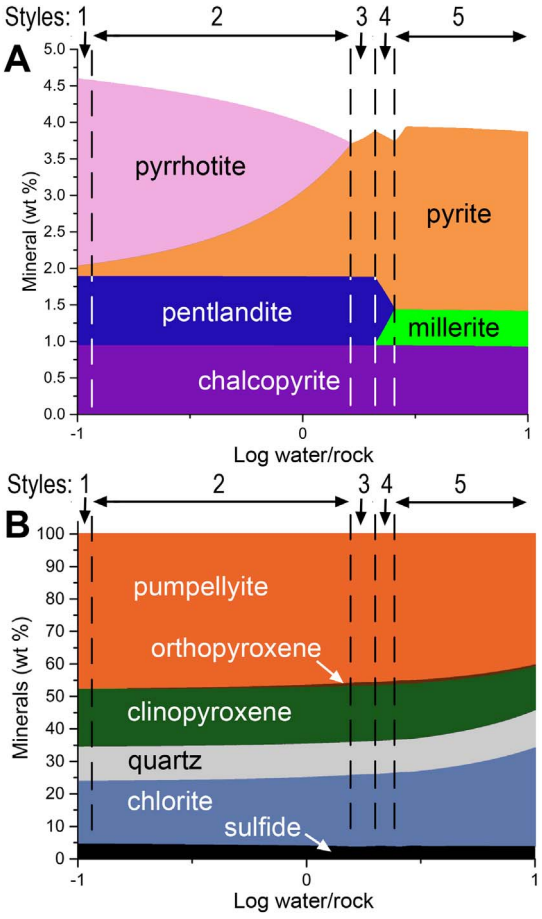

Fig. 11. CHILLER modelling of PMC alteration at 200 °C, showing the assemblages formed at Log water/rock ratios between −1.0 and 1.0. A: sulfide assemblage; B: silicate assemblage.

identified in general terms in previous studies of some magmatic sulfide deposits (Smith et al., 2011; Djon and Barnes, 2012; Duran et al., 2015; Piña et al., 2012, 2016), we have been able to quantify the mineralogical and geochemical changes during PMC alteration for the first time. Furthermore, a significant implication of our work is that PMC alteration involves significant mobilisation and loss of base and precious metals such that it produces hydrothermal fluids that may contain appreciable Ni, Cu and Pd. Our quantitative approach has demonstrated the following bulk losses and mineralogical transformations (Fig. 12):

- Early loss of pyrrhotite, which reduces the bulk sulfide volume by over 50%.
- Mid-stage recrystallization involving pentlandite to millerite and pyrrhotite to pyrite which involves further minor bulk losses.
- Copper loss throughout, but most pronounced in the final stage, which introduces some cubanite after chalcopyrite.
- Nickel is mobilised throughout the alteration, with some recrystallized from pentlandite to millerite, but a significant proportion is removed.
- Overall mass loss in the most advanced alteration styles is between 70 and 90%.
- Magnetite is not a significant alteration product.
- Palladium remains in pentlandite, increasing in tenor in decreasing volumes of pentlandite, but is expelled when pentlandite is lost and is not taken up by any other sulfides.
- The IPGE, Rh and Bi are taken up by the alteration products of their original hosts, being effectively transferred from pyrrhotite and pentlandite to pyrite and millerite and thus tenors increase as alteration progresses.

10.1. Characterisation of the PMC alteration process

The evolution of mineralogical proportions in the varying stages can be visualised on ternary phase diagrams. We use the elemental proportions shown in Fig. 4 and Table 2, to project those compositions onto the low temperature fields of the ternary Fe-Ni-S (Fig. 13A) and Fe-Cu-S (Fig. 13B) systems. In the Fe-Ni-S system at 100–135 °C (based on natural assemblages rather than experiments as the reaction rates are too slow; Naldrett 2011), PMC shows an overall progression from a typical magmatic sulfide assemblage of pyrrhotite-pentlandite to a more S-rich (pyrite) and Ni-rich (millerite) composition, which reflects the major Fe-loss relative to S and Ni (Fig. 5B). The five styles plot in fields that exactly match the observed mineralogy in our samples, illustrating that our observations are highly consistent with the established phase relations at low temperatures. In the Fe-Cu-S system (shown at 200 °C: the lowest temperature experimentally derived by Yund and Kullerud, 1966), the composition evolves from a typical magmatic sulfide composition of pyrrhotite-chalcopyrite to a more S-rich (pyrite) composition, with the disappearance of pyrrhotite in Style 3 shown by the composition plotting on the chalcopyrite-pyrite tie line. Styles 4 and 5 also plot close to this tie line, reflecting their pyrite-chalcopyrite assemblage although the observed minor increase in cubanite in the final stages is not consistent with the phase relations, which predict mostly chalcopyrite-pyrite together with bornite, covellite or digenite (Fig. 13B). This discrepancy is likely to be due to experimental constraints whereby Yund and Kullerud (1966) did not determine chalcopyrite-cubanite solid solutions below 400 °C. What can be show, however, is that Style 5 shows an increase in S and Fe and a decrease in Cu from Styles 3 and 4, as would be expected if chalcopyrite (CuFeS2) is replaced by cubanite ($CuFe_2S_3$).

The major loss of Fe during PMC alteration (Fig. 5B) is entirely consistent with the alteration of pentlandite ($(FeNi)_9S_8$) to millerite (NiS), and also the change from pyrrhotite (Fe_8S_9) to pyrite (FeS_2). The latter transformation could be explained by an addition of S, however, our data show this cannot be the case, and significant S is lost, alongside a considerable amount of Fe. Furthermore, the S/Se ratio work of Smith et al. (2016) also demonstrated that the secondary alteration involves a loss of S (and a subsequent increase in PGE tenor and reduction in S/Se ratio). Due to the lower mobility of Cu, Ni and the PGE compared with Fe and S, the process also increases the Cu, Ni and PGE tenor of the sulfides in the early-middle stages of PMC alteration, though the mobility of Cu is such that this is lost preferentially to Ni. The result of this is that, according to our data, the Ni tenors in sulfide increase by around three times by Style 4, and Cu tenors by ~0.3 times, though both reduce slightly in the most altered style.

Whilst increasing the tenor of the sulfides, PMC alteration does not necessarily increase bulk rock grades, with the sulfides being upgraded in some metals, but in increasingly smaller volumes in bulk rock (Fig. 12); thus the bulk rock grade may remain unchanged or actually *reduce* due to PMC alteration. The bulk rock data presented by Smith et al. (2014) shows that grades are highly variable in the GNPA and there is no systematic relationship between grade and sulfide texture. Furthermore, all pyrite-bearing assemblages are characterised as one in the work of Smith et al. (2014) and so the distinction between Styles 2–5 is not clear. Therefore, we are unable to show to what extent alteration actually affects bulk rock grade, though we do advocate increases in sulfide tenor. As such, the effects of PMC alteration have the most important implications for metallurgy (increased tenors; more complex mineralogy), rather than exploration or mining (possibly decreased bulk rock grades).

The tenors of the immobile IPGE and Rh increase by around ten times (and thus imply a reduction of sulfide by up to 90%; Fig. 7). Palladium increases in tenor by around ten times as long as pentlandite remains in the assemblage, but notably the final style has very little Pd in the sulfides, though it may be present as PGM, rather than being lost from the ore assemblage totally. The increase in PGE tenor in many of

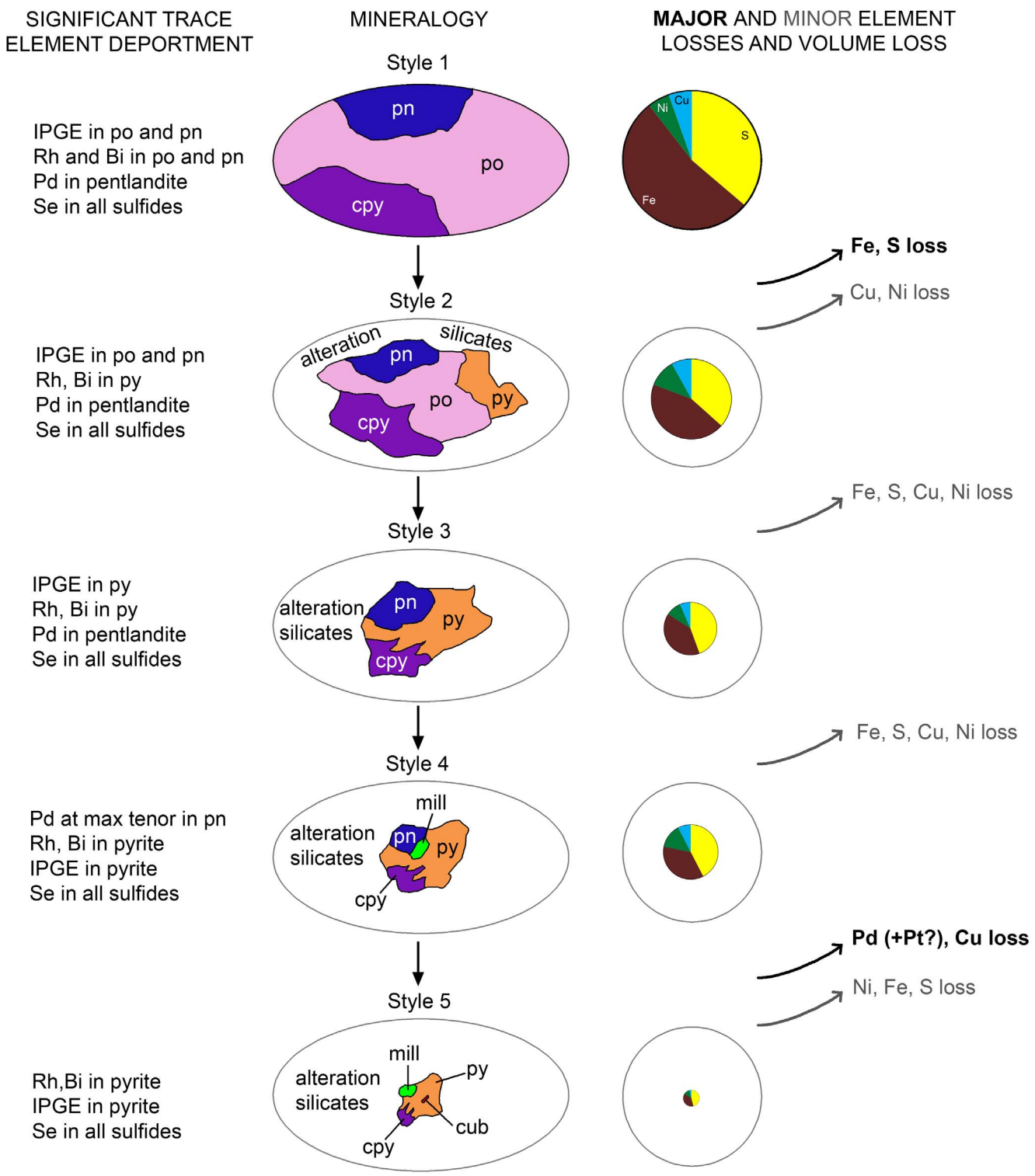

Fig. 12. Summary of mineralogical and geochemical changes during PMC alteration. Abbreviations: pn = pentlandite, po = pyrrhotite, cpy = chalcopyrite, py = pyrite, mill = millerite, cub = cubanite.

the sulfides indicates that during PMC alteration, some elements are effectively retained in increasingly smaller volumes of sulfide (e.g. Pd in pentlandite) or transferred effectively to alteration products (e.g. IPGE from pyrrhotite to pyrite). Pyrite, millerite and chalcopyrite are intergrown in the latter styles (Fig. 2L,O) illustrating that recrystallization during alteration produces texturally complex, as well as upgraded, ores. Fig. 12 illustrates schematically the mineralogical changes, elemental transfers and mass losses through the process of PMC alteration.

We do not include Pt in our calculations and modelling due to it largely being present as PGM, which are generally too small to fully constrain quantitatively with the Mineralogic analysis, thus we do not have the quantitative data for the end member Style 1. That said, it is worth noting at this point that in many hydrothermally altered magmatic sulfide deposits, pyrite has been identified as a major host for Pt (e.g. Dare et al., 2011; Piña et al., 2012; Djon and Barnes, 2012; Graham et al., 2017). Smith et al. (2014) report Pt contents for

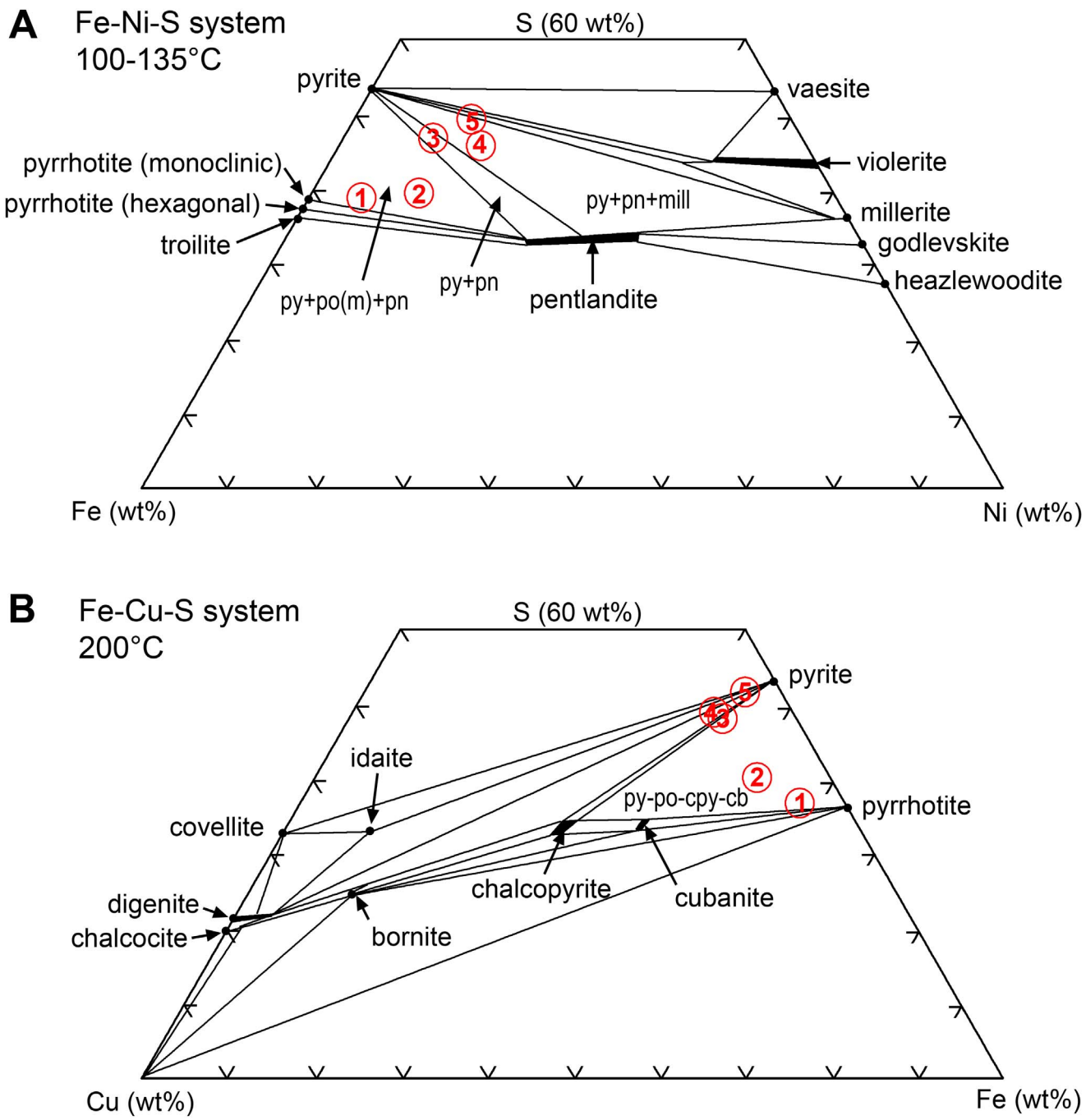

Fig. 13. A: Ternary phase diagram for the Fe-Ni-S system at 100–135 °C (after Naldrett, 2011), showing the position of the PMC alteration styles. B: Ternary phase diagram for the Fe-Cu-S system (after Yund and Kullerud 1966) showing the position of the PMC alteration styles.

secondary pyrite in the GNPA Member up to 63 ppm. As we are unable to quantify the mass balance for Pt, we assume that some is taken up in pyrite, some held within PGM (as shown by Smith et al., 2014), but there is the possibility that some is also lost along with the Ni, Cu and Pd, which can be tested by assessing the bulk rock data.

It is important to note that our approach focusses on the sulfide portion of the rocks, whereas Smith et al. (2014) presented bulk rock data as well as sulfide LA-IPC-MS and PGM data from the same GNPA samples we have used. Interestingly, bulk rock Rh/Pt ratios are consistent between their 'primary' and 'secondary' assemblages, implying that Pt has similar behaviour to Rh. Although some Rh is present as PGM; hollingworthite is present in both primary and secondary assemblages; Smith et al., 2014), the majority is present within the sulfides (demonstrated by the mass balance in Smith et al., 2014), and is largely immobile. The mass balance of Smith et al. (2014) shows that almost all the Pt is present as PGM with only a minor amount held in secondary pyrite. The consistent bulk rock Rh/Pt ratio would thus imply that Pt has a similar mobility under PMC conditions to Rh, and as we show that Rh is highly immobile, we infer that Pt may not be significantly mobilised during PMC alteration and is present largely as Pt-bearing PGM.

PMC alteration is distinct from actinolite-tremolite-talc (amphibolite) alteration that is extremely common in magmatic sulfides (Li et al., 2004) in that the alteration minerals differ and during this style of amphibolite alteration, the sulfide assemblages are rarely altered to pyrite and millerite. Similarly, it is not serpentinisation, as we see no serpentine, there is no olivine in the GNPA Member to start with, and no significant magnetite is produced. The nature of any alteration

assemblage will be a product of the composition of the fluid involved in the alteration, the fluid conditions, as well as the minerals that react during alteration. Incompatible elements like Cu, S and Pd would not be expected to be present in secondary silicate assemblages, and are assumed to have been mobilised, though some Fe and perhaps Ni may be incorporated in some secondary silicates; however no trace element data for the silicates is available. All of this means that after up to 90% alteration of the sulfide assemblage, these elements have been mobilised into a hydrothermal fluid that subsequently will have contained elevated Ni, Cu, Pd and S.

10.2. Modelling the PMC alteration process

The results of the hydrothermal reaction-path modelling (Fig. 11) produce a sulfide assemblage that approximates the five Styles observed in the natural samples, organised in progressively increasing water rock ratio (w/r). The model demonstrates that re-equilibration of the sulfide assemblage with a moderate temperature (200 °C) hydrothermal fluid can account for the observed sulfide styles. Furthermore, the modelling also confirms our visually determined progression in styles in terms of sulfide mineralogy. It is worth noting, however, that Styles 3 and 4 occupy very small windows in the w/r range compared with Styles 2 and 5. The style boundaries have Log w/r values of approximately −1, 0, 0.5, 0.6 and 0.7 (Fig. 11). As such, our five styles are not equal in terms of w/r and thus as a 'measure' of alteration, do not represent equal ranges of w/r. This probably accounts for some slightly unusual features like the flattening of the Rh ratio plot at Styles 3 and 4 in Fig. 10, which depicts each style equally along the x axis.

The heated seawater used as the synthetic hydrothermal fluid in the model will have some control over the final assemblages observed in the model outputs, particularly the silicate mineralogy, but in the absence of any control over the nature of the actual hydrothermal fluid driving PMC alteration in the GNPA Member, we consider the heated seawater to be a conservative proxy with a range of cations and anions typical of generic hydrothermal fluids. At the low w/r values used in the interpretation, the hydrothermal assemblage is strongly controlled by the rock assemblage rather than the fluid (Reed, 1997; Smith et al., 2017), and thus the uncertainties about the nature of the fluid are outweighed by the well constrained original rock assemblage. The fluid is contributing H_2O and anions (Cl^-, SO_4^{2-}, HS^- and HCO_3^-). At the rock-dominated equilibrium, pH is near-neutral, consistent with rock equilibration at moderate salinity (Reed, 1997; Giggenbach, 1997). Redox is controlled by the sulfide component of the rock and the bulk rock Fe^{2+}/Fe^{3+} and hence sulfate/sulfide and ferrous/ferric minerals (Reed, 1997). For lower total sulfide content in the rock, system fO_2 will be increasingly controlled by fluid fO_2.

The cation composition of the rock will dominate the cation composition of the fluid, notwithstanding the solubility of certain cations and cation complexes at 200 °C (e.g. aqueous Mg is low; Giggenbach, 1988). As we have a perfect understanding of the original rock composition, the inputs to the model in this respect are highly constrained as being a plagioclase-orthopyroxene-clinopyroxene-sulfide(-chromite) mixture. The hydrothermal fluid has a greater influence over the bulk hydrothermal composition with respect to elements which are less abundant in the initial GNPA Member bulk rock composition, particularly Na and K. Alteration minerals containing Na and K (e.g. phlogopite) are thus poorly constrained in the model, as they are controlled by fluid cation composition across all w/r. This explains the mismatch between the observed and modelled alumina-silicate assemblage: the model results include pumpellyite (Fig. 11B), whereas the observed alteration actually contains K-bearing phlogopite and sericite (Fig. 9). Allowing for this, the rest of the silicate assemblage as predicted by the model matches the observed mineralogy well, with quartz, chlorite and two pyroxenes.

Hydrothermal re-equilibration and recrystallization of the sulfide minerals during PMC alteration means that trace elements can partition between the equilibrium phases, resulting in the preferential concentration of Pd in pentlandite (Fig. 8A). Nickel and Cu are relatively conservative in the sulfide phase; Fe and S loss to the fluid and, for Fe, the silicate assemblage is the main mechanism by which the total sulfide assemblage mass decreases. There is, however, a significant discrepancy between the modelled volume loss and that calculated from the textural information (Fig. 9) and the sulfide Rh tenor data (Fig. 10). The modelling predicts a volume loss from the sulfide portion, but of the order of around 10%, whereas the Rh (and Bi) data, and the textural interpretations indicate up to 90% volume loss of sulfide.

The modelling has a number of inherent assumptions and constraints which mean that there will always be some inconsistencies expected. As discussed above, system fO_2 is strongly controlled by rock Fe^{2+}/Fe^{3+} and total sulfide. In the situations where the altered volume of rock has < 5 wt% total sulfide minerals (lower than that modelled), then the progressive loss of sulfides through oxidation may be proportionally greater, which may account for some the discrepancy in volume change between the observed and modelled results. Secondly, the interpretation of the original sulfide boundaries as exemplified in Fig. 9 may not be accurate if the hydrous silicates represent, at least in part, trapped pockets of differentiated and volatile rich melt, as well as, some secondary replacement. Nevertheless, the order of magnitude increase in Rh tenors and Pd tenors up to Style 4 are more difficult to explain other than significant volume loss of sulfide of up to 90%. Therefore, with the two independent textural and geochemical relationships consistent, we favour large volume loss greater than the modelling predicts.

10.3. Hydrothermal mobility of base, precious and semi-metals

One of the most significant implications of our study is the demonstration that *all* of the major components of the sulfide assemblage; Cu, Ni, Fe and S, are mobilised during PMC alteration. It is not surprising that Fe and S are the most mobile, and there are many examples where Cu, along with Au, show elevated mobility relative to Ni and PGE (e.g. Lac des Iles, Boudreau et al., 2014; River Valley, Holwell et al., 2014; Kevitsa; Le Vaillant et al., 2016b) but the significantly mobile behaviour of Ni and PGE are relatively uncommon, and so provide important constraints on fluid composition and conditions of PMC alteration.

Nickel is one of the least mobile base metals in hydrothermal fluids, but Liu et al. (2012) demonstrate that it is soluble as chloride complexes at low temperatures (< 250 °C; consistent with PMC alteration temperatures). Liu et al. (2012) show that Ni can be dissolved from pentlandite and millerite by the following reactions:

$$NiS_{(millerite)} + H^+ + xCl^- = NiCl_x^{2-x} + HS^- \quad (1)$$

$$Fe_{4.5}Ni_{4.5}S_{8(pentlandite)} + 10H^+ + 4.5(x+y)Cl^- = H_2(aq) + 8HS^- + 4.5NiCl_x^{2-x} + 4.5FeCl_y^{2-y} \quad (2)$$

From these reactions, Liu et al. (2012) interpret that the solubility of millerite is redox-independent in the predominance field of HS^- whereas the solubility of pentlandite increases with increasing fO_2. Furthermore, at high fO_2, both minerals are soluble due to the predominance of the oxidised S species. Given the fact that pentlandite is completely dissolved in PMC alteration, and that millerite volume also decreases (Fig. 12), we infer that the fluid conditions that affected the GNPA member rocks were highly oxidising. And furthermore, the mobilised Ni was most likely transported as Ni (II) chloride complexes. Note that Fe is also mobilised as a chloride complex in (2). Liu and McPhail (2005) demonstrated that Cu can also be mobilised as Cu (I) chlorides across a wide temperature range, and different deposit types. As such, Fe, Ni and Cu can conceivably be mobilised and transported in oxidised, acidic fluids as chloride complexes.

It appears that Pd becomes mobile from sulfide in the final stages of

alteration, though the fate of it is unclear. Palladium is known to be mobile in hydrothermal fluids as chloride complexes in unusually acidic and oxidised conditions and as bisulfide complexes in acidic and reduced conditions (e.g. Mountain and Wood, 1988; Wood, 2002; Barnes and Liu, 2012). Thus Pd mobility is indicative of acidic fluids. From the oxidising conditions implied by Eqs. (1) and (2), we propose that the fluids that interacted with the GNPA Member sulfides were both acidic and oxidising, and may have mobilised some Pd as chloride complexes along with the base metals. Furthermore, it is possible that this process also mobilised Pt as Barnes and Liu (2012) state that both Pt and Pd can be mobilised as chloride complexes under extremely acidic and oxidising conditions. However, as discussed above, the good bulk rock correlation between Rh and Pt in all styles (Smith et al., 2014) would imply that Pt mobilisation is minimal, and thus the fO_2 and pH conditions may not have been extreme.

At this point, it is pertinent to assess the modelling results and alteration style based on this interpretation of oxidised and acidic fluid interaction with the sulfides. An initially oxidised, acidic fluid may be important for the mobilisation of e.g. Ni, Cu and Pd, but the final mineral record after their re-precipitation is of a more reduced, pH neutral fluid: i.e. one that has reacted and equilibrated with the host rock. The modelled compositions of the secondary assemblages are consistent with low w/r conditions, and an equilibrium point much closer to the rock than the initial fluid. The abundance of anhydrous, primary silicates in the samples support the relatively low amounts of alteration. A more oxidised and acidic fluid than the modified seawater used in the modelling would be expected to react more aggressively, and may be responsible for the greater volume loss in observed samples compared to the models. However, the observed mineral assemblage is consistent with modelled mineralogy at low w/r, indicating that the flux of fluid was small, though evidently effective at mobilising metals.

The behaviour of the two semi metals we present data for contrast significantly. Bismuth shows remarkably similar trends to Rh, increasing in concentration in the sulfides as alteration progresses; consistent with fairly immobile behaviour during PMC alteration. In contrast, Se tenors indicate that whilst there is a slight overall increase in tenor as alteration progresses, this is nowhere near that of the more immobile IPGE, Rh and Bi (Fig. 8). Therefore there is some bulk Se loss during PMC alteration, though this is not as great as the loss of S. This is perfectly in line with the findings of Smith et al. (2016) who recognised a reduction in S/Se ratio alongside an increase in Pt + Pd tenor as a function of alteration, and highlights that hydrothermal activity reduces S/Se ratios. In terms of the nature of the fluids that mobilise Se, Prichard et al. (2013) propose that Se, along with Pd, can be mobilised from base metal sulfides at low temperatures (100–300 °C) in highly oxidising and acidic conditions, though in their case study at Jinchuan, China, significant magnetite was produced as a product of alteration.

The Cu and Ni that are lost during PMC alteration are not re-precipitated as major elements in any other phases in the GNPA Member rocks we studied and are therefore considered to be mobilised effectively into a fluid phase. It is possible some may be incorporated into secondary silicates in trace amounts, but whilst this may account for some of the bulk metals, the majority must have been lost to a fluid phase. The alteration of Pd-bearing pentlandite is also likely to mobilise Pd, however, there remains the question as to whether Pd and Pt are fully transferred into the fluid phase or simply recrystallized to secondary PGM. Whereas Pt and Rh show a good bulk rock correlation (Smith et al., 2014) inidicative of similarly immobile behaviour and the presence of Pt as PGM, there is a very weak bulk rock correlation between Rh and Pd, which would support divergent behaviour. If all the Pd was recrystallized to PGM, then the bulk rock Rh/Pd ratio should stay the same, but this is not the case. Smith et al. (2014) document that the most altered assemblages still contain Pd- and Pt-PGM, including an increase in Pd-antimonides associated with secondary silicates (usually considered indicative of fluid activity; Holwell et al., 2014), though the proportion of Pd to Pt minerals by area decreases from primary to secondary assemblages. As such, not all Pd is lost to the fluid phase, but this does back up preferential loss of Pd over Pt. We therefore suggest that PMC alteration mobilises Fe, Cu, Ni, Pd, Se and S into hydrothermal fluids, and that the IPGE, Rh and Pt remain relatively immobile.

There are few studies on the hydrothermal remobilisation of Ni, Cu, Co and PGE from Ni-Cu-PGE sulfide deposits, however, Le Vaillant et al. (2015, 2016a) identified hydrothermal haloes around Ni-sulfide orebodies and provided a number of insights into the possible sources and compositions of fluids. They show Ni, Co and PGE remobilisation in a geochemical halo up to 1780 m away from the Sarah's Find massive sulfides, in the Yilgarn Craton and proposed, due to the gersdorffite-dominated alteration mineralogy, that As-rich fluids related to a regional orogenic gold event were responsible for mobilisation. Whilst this does confirm that Ni, Co and PGE are hydrothermally mobile under certain conditions, the mineralogy of the Sarah's Find massive ores are pyrrhotite-pentlandite-chalcopyrite rather than being pyrite-millerite-dominated. In addition, we have no evidence of the mineralogy of any redeposited Ni-bearing minerals in our Bushveld case study, so there is no direct evidence for an analogous fluid process to that we describe. Furthermore, orogenic gold-related fluids are characteristically near-neutral pH, slightly reduced, and dominated by sulfide complexes (Goldfarb et al., 2005). This contrasts to the acidic and oxidising conditions that are more consistent with the element mobility we record and thus this is not an example of PMC alteration but does, nevertheless, indicate that there may be multiple conditions whereby Ni-Cu-PGE may be hydrothermally remobilised from primary magmatic ores.

At Kevitsa, Finland, Le Vaillant et al. (2016b) demonstrate that hydrothermal remobilisation by serpentinisation, amphibolitisation and epidotisation significantly mobilises Cu and Au. However, Ni and the PGE remain relatively immobile, though some redistribution of Ni is shown on a millimetre scale in some vein selvages. The processes of serpentinisation and metamorphism are very common in many mafic-ultramafic hosted Ni-Cu-PGE deposits, but are notably absent from our GNPA Member samples and these common processes appear to have little effect on Ni and PGE mobility. Serpentinisation involves fluids that are alkaline and reduced (Hulbert et al., 1988), in direct contrast to the evidence discussed above, and thus we conclude that serpentinisation has no relation whatsoever to PMC alteration.

Boudreau et al. (2014) describe progressive alteration of the Lac des Iles Offset Zone Ni-Cu-PGE sulfides that involves the formation of epidote/clinozoisite, chlorite, amphibole, quartz muscovite/sericite, calcite and late talc after amphibole. This study used a different approach to ours; silicate mineral mode calculations, but came up with a similar conclusion that some base and precious metals were mobilised into a hydrothermal fluid. There are some differences in style however, with the alteration assemblage being amphibole rich, whereas ours is poor in amphibole, and the sulfide assemblage that Boudreau et al. (2014) record is low in millerite. This latter characteristic may be due to the proposed fluids being higher temperature (~350–450 °C; Boudreau et al., 2014). Furthermore, the Lac des Iles alteration mobilises S, Cu, Pt and Au, but not significant Ni and only some Pd. This may not be PMC alteration, but it still shows that base and precious metals can be mobilised from magmatic sulfides. This study of Boudreau et al. (2014) goes a step further and suggests that the metals mobilised from this alteration were channelled along fault zones and may have been a source for the high temperature hydrothermal Cu-Au-PGE New Rambler deposit,

In summary, we propose that PMC alteration is not serpentinisation, or amphibolitisation, but is a distinct process that involves highly acidic and oxidising conditions at low temperatures (probably around 150-200 °C), which mobilises S, Fe, Ni and Cu, plus Pd (and probably Au); most likely as chloride complexes.

10.4. A source for hydrothermal Pt and Pd deposits?

As discussed above, Boudreau et al. (2014) have shown that Pt and Pd along with S, Cu and Au can be mobilised and potentially form high temperature hydrothermal PGE deposits. The potential for PMC alteration to mobilise Pd is clear (though Pt may be much less mobile in these conditions) and it follows that the low temperature fluids involved in PMC alteration may provide a source for other hydrothermal Pd deposits. Sener et al. (2002) describe a number of epigenetic, structurally controlled, sulfide-poor, Au-Pt-Pd vein deposits at Gold Ridge and Coronation Hill, Australia, and Serra Pelada, Carajas region, Brazil, that they propose were formed from low temperature (< 300 °C) saline and acidic fluids with metals transported as chloride complexes. This is consistent with the fluids we propose are responsible for PMC alteration, however Sener et al. (2002) proposed the source of metals for Serra Pelada to be related to alkaline magmatism that also formed the large Iron-Oxide-Copper-Gold deposits of the Carajas region. However, there are mafic-ultramafic rocks in the region that offer the alternative possibility of a PMC alteration source.

Perhaps though, the most intriguing hydrothermal PGE deposit of all is the Waterberg hydrothermal Pt deposit, 15 km west of Mookgophong in northern South Africa. What makes this worthy of discussion in relation to our study is its close proximity to the GNPA Member (Fig. 14A) which we propose as the 'type locality' for PMC alteration. The Waterberg hydrothermal Pt deposit (not to be confused with the sedimentary Waterberg Group, or the newly discovered Waterberg Ni-Cu-PGE deposit in the far northern limb of the Bushveld Complex) is a structurally controlled Pt-quartz vein deposit. The fluids are proposed to have been highly oxidised and acidic in order to initially transport the Pt as chloride complexes. They remained highly oxidised but were modified by fluid-rock reactions to more neutral pH at the site of deposition (McDonald et al., 1995, 1999). Armitage et al. (2007) proposed that a possible source of the Pt were tectonic slivers of PGE-rich mafic bodies from the northern limb of the Bushveld Complex present along the Welgevonden-Planknek Fault network (WPF; Fig. 14B); splays from which host the Waterberg Pt veins. It is interesting to note that among the known northern Bushveld Complex Ni-Cu-PGE deposits, PMC alteration is only prevalent in the GNPA Member and not the Platreef further north (e.g. McDonald and Holwell, 2011; Fig. 14A) or the Volspruit Sulfide zone (e.g. Hulbert and von Gruenewaldt, 1982), hosted by the Lower Zone stratigraphically below the GNPA Member (Fig. 14A).

Spatially, the GNPA member is located adjacent to the WPF (Fig. 14B), and thus potentially provides a direct conduit for fluids from the GNPA Member to the Waterberg deposit. However, there are two main arguments against this link; the first of which is the metal budget. PMC appears to produce Ni-Cu-Pd-rich fluids, yet the Waterberg is a Pt-only deposit. Secondly, there is a chronological constraint on this proposed link as the Waterberg veins cut host sandstones of Triassic age (the Clarens Formation) and are interpreted to be the most recent event in the area (< 180 Ma), based on structural mapping by Armitage et al. (2007). The timing of PMC alteration of the GNPA member is not clear, but is assumed to be late magmatic, though could conceivably be much more recent. If there is a clear chronological gap between PMC alteration and Waterberg Pt mineralisation (possibly up to 1900 Ma), then any linkage would require an intermediate deposit, for example as a hydrothermal Ni-Pt-Pd deposit somewhere along the WPF (Fig. 14B), that is then remobilised at a later stage, with further fraction of Pt from Pd and the base metals, to form the Pt-rich veins. Whilst this may seem unlikely, the uniqueness of the Waterberg deposit may attest to very unusual circumstances in its genesis. Nevertheless, the spatial correlation between the poorly understood Waterberg and a large mafic-ultramafic body that has undergone PMC alteration remains tantalising.

10.5. A source for hydrothermal Ni deposits?

The fate of the fluids that mobilise Cu, Ni, Pd (and probably Au) from a magmatic sulfide assemblage during PMC alteration represent metal-rich fluids with the potential to form hydrothermal base metal ore deposits. The studies of Le Vaillant et al. (2015, 2016a) show that the elements may be remobilised and dispersed in a hydrothermal halo, but the alternative may be that they could concentrate the elements into secondary hydrothermal deposits. There are few hydrothermal ore deposits that contain Ni-Cu-Pt-Pd, with the exception of the New Rambler deposit referred to earlier (Nyman et al., 1990; Boudreau et al., 2014) but there are some examples of unusual hydrothermal Ni deposits (with some Cu, Pt, Pd and Au) where the source of metals is controversial (González-Álvarez et al., 2013).

The Avebury Ni deposit in Tasmania is a hydrothermal Ni deposit hosted by ultramafics within an ophiolite sequence. Keays and Jowitt

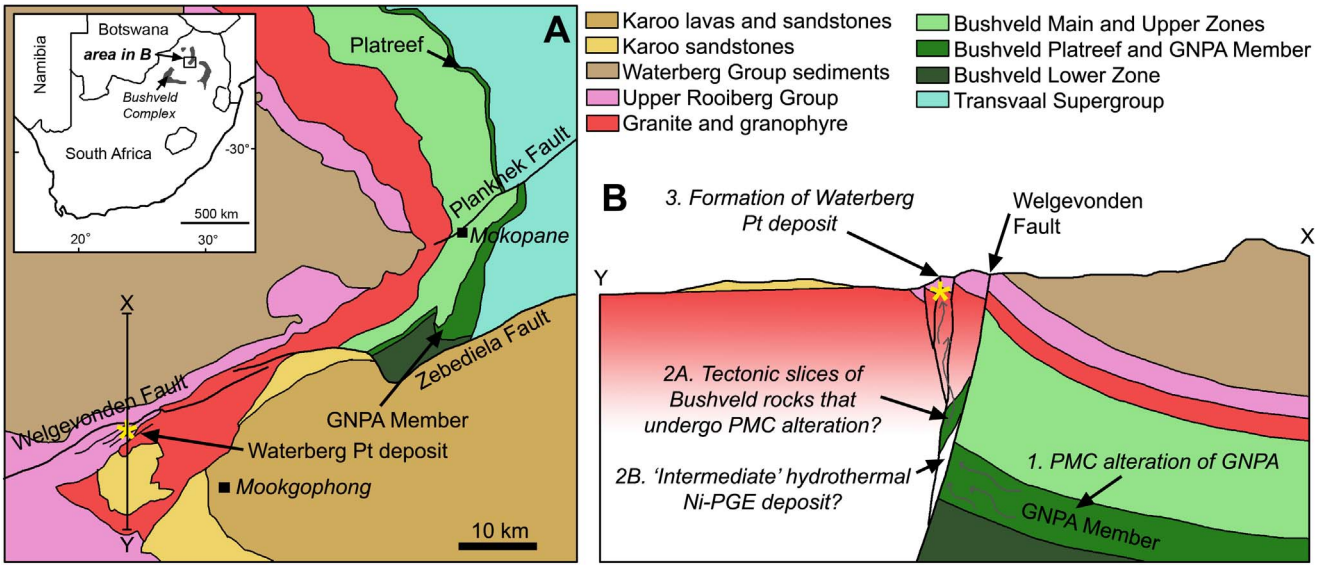

Fig. 14. Possible relationship between the GNPA Member and the Waterberg Pt deposit. A: Geological map of the Mookgophong-Mokopane area of northern South Africa showing the location of the GNPA member in the northern limb of the Bushveld Complex, and the Waterberg Pt deposit. The Welgevonden-Planknek and Zebediela Faults are major deep crustal lineaments. B: Cross section (as shown in A) across the Welgevonden Fault. The GNPA Member is at depth on the northern side of the fault. The possible link between the two deposits is illustrated through stages numbered 1–3. Modified after Armitage et al. (2007).

(2013) rule out the possibility that the largely pentlandite-rich ores were formed from in situ metasomatism of magmatic sulfides due to poor negative correlations between Ni and the IPGE and Rh. Instead, they suggested the Ni, Pd, Au and Cu bearing nature of the ores was a result of the mobilisation of these elements from magmatic sulfides elsewhere in the system. This would be entirely consistent with a process of alteration as shown by our study, with IPGE, Rh and Pt immobile in the remaining original, sulfide assemblage and Ni, Cu, Pd and Au mobilised and deposited distally in a hydrothermal deposit. As such, it represents possibly the best potential candidate for a remobilised Ni-sulfide deposit formed as a result of PMC alteration.

Two hydrothermal Ni deposits with less well constrained metal sources are the Enterprise Ni deposit in the Copperbelt of Northwestern Province, Zambia, and Talvivarra in Finland. Enterprise is a sediment-hosted, hydrothermal Ni deposit with elevated Cu, Co and PGE, and a zone of Cu-rich mineralisation stratigraphically below the main Ni mineralisation (Capistrant et al., 2015). The source of Ni is not known, and whilst Capistrant et al. (2015) do note that there are metagabbros in the basement rocks at Enterprise, they are volumetrically small and are not known to contain sulfides. Nevertheless, the mobilisation of Ni, Cu, Pt and Pd from magmatic sulfides from an unidentified source in the region remains a possibility for the source of metals at Enterprise. The black shale-hosted Talvivarra hydrothermal Ni-Cu-Pb-Zn deposit in the Outokumpo region, Finland, is associated with talc-rich rocks interpreted to be altered serpentinites. Loukola-Ruskeeniemi and Lahtinen (2013) suggest that the large concentrations of Ni at Talvivaara were sourced from ultramafic rocks, but do not specify the exact mechanism.

The Epoch Ni sulfide deposit in the Filabusi Greenstone Belt of southern Zimbabwe is a pyrite-millerite-chalcopyrite-pentlandite-magnetite deposit hosted by sheared talc-carbonate rocks of ultramafic protolith (Pirajno and González-Álvarez, 2013). The mineralogy is interesting as it is comparable to PMC altered magmatic sulfide deposit, though notably magnetite is much more common, and forms up to 48% of the ore assemblage. Pirajno and González-Álvarez (2013) proposed that the deposit was hydrothermal in origin, but with a complex fluid history of serpentinisation, carbonatisation and talc-carbonate alteration, could not constrain exactly whether the mineralisation was a metasomatised magmatic sulfide deposit, or a fully mobilised hydrothermal deposit. It may be that it represents an ultramafic hosted Ni-Cu-PGE deposits that has undergone PMC alteration, or potentially, the result of the deposition of Ni-Cu-PGE-rich fluids from PMC alteration elsewhere.

As the examples above show, ultramafic-mafic rocks with or without magmatic sulfides have been tentatively suggested as metal sources for several enigmatic hydrothermal Ni deposits. We note that PMC alteration is a relatively unusual style (c.f. common actinolite-tremolite-talc replacement; Li et al., 2004) and is evidently uncommon. This may, however, be consistent with such alteration being a source for hydrothermal Ni deposits, which are also relatively rare. In order to prove this link, evidence of source rocks with residual pyrite-millerite-chalcopyrite assemblages in the vicinity of hydrothermal Ni deposits would need to be identified, similar to the link Boudreau et al. (2014) made between the Lac des Iles and New Rambler deposits. Nevertheless, our data proves that Ni, Cu and Pd can be effectively and significantly mobilised into a fluid phase from the alteration of a magmatic sulfide assemblage. Furthermore, we demonstrate that the mass losses from the magmatic sulfide are significant (up to 90%) and therefore do represent a viable source of the volumes of metal required to produce subsequent hydrothermal deposits.

10.6. Wider implications for metal transfer in ore systems

A number of studies over the past decade have quantitatively addressed the subject of sulfide (and other mineral) transformation and mobilisation of metals as sources for a variety of ore deposits, through mass balance calculations. Examples include Pitcairn et al. (2010), who studied minor sulfides present in the metamorphic rocks of the Otago and Alpine schists, New Zealand and showed that during metamorphism, Pb, Zn and Co are retained in the rock, incorporated into other minerals, whereas As, Sb, Hg, Au, and Ag are removed from the rock. The latter being an important proposed source of metals for orogenic Au deposits, as originally proposed by Pitcairn et al. (2006). Sulfides are not the only known mineral source that can subsequently provide metals to hydrothermal fluids during alteration. Cave et al. (2015, 2017) quantitatively show that the breakdown of rutile and titanite are sources for W mineralisation in the Otago schists of New Zealand, and mass balance calculations by Patten et al. (2016) estimate the volumes of lower oceanic crust required to be altered to provide the metals in volcanogenic massive sulfides. These studies have thus been able to quantify the volumes of low grade crustal material required to form ore deposits by mobilisation of metals within hydrothermal fluids. As the first study of its kind on the transformation of magmatic Ni-Cu-PGE sulfides, our work adds to this increasing breadth of quantitative knowledge on the sources of metal-rich fluids and, in contrast to the other works cited above, demonstrates that the reworking of existing ore deposits and subsequent fractionation of metals during fluid transport are also viable sources for some hydrothermal ore deposits.

11. Summary

Through the application of quantitative, automated mineralogy, alongside LA-ICP-MS analysis, we have been able to characterise the mineralogical changes and element deportments, gains and losses during a progressive process of alteration. Our quantitative mineralogy is consistent with both textural observations and modelling of the hydrothermal alteration stages of a primary magmatic pyrrhotite-pentlandite-chalcopyrite assemblage at low temperature (~150–200 °C) to pyrite-millerite-chalcopyrite. The PMC alteration process initially increases the Cu and Ni tenors by removing the bulk of the Fe and S at an early stage, however, Ni and Cu are mobilised during PMC alteration and are lost as water-rock interaction continues. The fluids responsible were most likely to have been acidic, oxidised, and metals mobilised by as chloride complexes. Most chalcophile trace elements however remain in the sulfides, meaning that the most altered sulfide assemblages, whilst of lower volume have very high tenors of elements such as the IPGE and Rh, largely hosted by secondary pyrite. Overall, the PMC style of alteration differs from the more common alteration seen during serpentinisation and metamorphism in that Ni, and Pd as well as Cu are mobilised. A consequence of this low temperature hydrothermal alteration is that it produces fluids that are enriched in Ni, Cu and Pd, and which may provide a source for enigmatic hydrothermal Ni(-Cu-PGE) deposits.

Acknowledgments

Carl Zeiss Microscopy is acknowledged for access to Mineralogic software and SEM analysis and both technical and financial support of ZA's and LAW's MGeol projects. Samples for this study were obtained from Caledonia Mining Ltd. as part of JWS's PhD project, funded by NERC (NE/1528426/1). This work is part of a large project funded by NERC SoS Consortium grant NE/M010848/1 and NE/M011615/1 "TeaSe: tellurium and selenium cycling and supply" awarded to the University of Leicester and Cardiff University, respectively. Reviews by Margaux Le Vaillant and Charley Duran are gratefully acknowledged for providing constructive suggestions on improving the manuscript.

Appendix A

Table A1
Mean concentrations (ppm) of trace elements in sulfides from each Style of PMC alteration (From Smith, 2014).

		n	Se	Ru	Rh	Pd	Os	Ir	Pt	Bi
Po	Style 1	22	102.8	1.69	0.17	0.42	0.26	0.24	0.12	1.13
Po	Style 2	8	117.3	1.95	0.08	1.50	0.43	0.40	0.62	1.32
Py	Style 2	7	106.3	3.72	7.49	3.88	0.39	0.41	1.47	11.45
Py	Style 3	7	236.0	0.14	4.06	10.46	0.11	0.14	0.01	26.71
Py	Style 4	22	139.8	2.67	2.87	3.93	0.34	0.58	4.71	23.27
Py	Style 5	15	110.0	17.10	5.86	4.65	2.10	1.50	0.12	41.83
Pn	Style 1	9	97.7	3.95	0.46	10.38	0.50	0.15	0.10	2.61
Pn	Style 2	6	128.3	5.39	0.56	31.36	0.66	0.53	0.28	9.94
Pn	Style 3	7	156.3	1.52	0.57	61.73	0.38	0.11	0.03	4.85
Pn	Style 4	15	130.2	1.93	2.18	209.16	0.26	0.35	3.51	3.23
Mill	Style 4	7	114.3	0.56	0.66	0.92	0.20	0.53	0.33	2.47
Mill	Style 5	4	345.5	0.88	0.22	0.87	0.16	0.29	0.04	8.52
Cpy	Style 1	3	–	0.03	0.04	0.22	0.01	0.03	0.01	0.42
Cpy	Style 2	–	–	–	–	–	–	–	–	–
Cpy	Style 3	2	–	0.10	0.04	0.23	0.01	0.01	0.01	0.19
Cpy	Style 4	5	–	0.07	0.04	0.05	0.01	0.01	0.01	1.60
Cpy	Style 5	3	–	2.32	0.06	0.16	0.32	0.73	0.01	7.17
Cub	Style 1	7	96.0	0.05	0.06	0.18	0.03	0.07	0.03	0.47
Cub	Style 2	4	103.8	0.73	0.05	0.76	0.14	0.11	0.02	1.04
Cub	Style 3	2	138.0	0.03	0.05	2.61	0.02	0.01	0.35	1.60
Cub	Style 4	4	127.8	0.67	0.05	0.10	0.01	0.02	0.02	0.72
Cub	Style 5	4	81.8	0.09	0.05	0.30	0.02	0.01	0.02	0.82

Notes
No data for style 2 cpy; assumed to be same as Style 1 for purposes of tenor calculations.
No data for Se in Style 1 cpy; assumed to be same as Style 1 cubanite for purposes of tenor calculations.

Table A2
Trace element tenors (ppm) in each sulfide in each stage (for deportment calculation) – Fig. 8.

	Os	Ir	Ru	Rh	Pd	Bi	Se
Stage 1							
po	0.19	0.17	1.25	0.13	0.31	1.13	76.14
pn	0.06	0.02	0.48	0.06	1.27	2.61	11.94
cpy	0.00	0.00	0.00	0.01	0.03	0.42	12.72
cub	0.00	0.01	0.01	0.01	0.02	0.47	12.87
Stage 2							
po	0.16	0.15	0.72	0.03	0.56	1.32	43.67
pn	0.21	0.17	1.68	0.17	9.77	9.94	40.00
py	0.03	0.03	0.27	0.55	0.29	11.45	7.83
cpy	0.00	0.00	0.00	0.00	0.00	0.00	24.83
cub	0.00	0.00	0.00	0.00	0.00	1.04	0.30
Stage 3							
pn	0.09	0.03	0.37	0.14	15.02	4.85	38.03
py	0.06	0.08	0.08	2.26	5.83	26.71	131.70
cpy	0.00	0.00	0.02	0.01	0.04	0.19	25.31
cub	0.00	0.00	0.00	0.00	0.04	1.60	2.10
Stage 4							
pn	0.05	0.06	0.35	0.40	38.39	3.23	23.90
py	0.17	0.29	1.32	1.42	1.94	23.27	69.03
mill	0.02	0.05	0.06	0.07	0.09	2.47	11.46
cpy	0.00	0.00	0.01	0.01	0.01	1.60	27.11
cub	0.00	0.00	0.01	0.00	0.00	0.72	1.29
Stage 5							
py	1.44	1.03	11.73	4.02	3.19	41.83	75.49
mill	0.03	0.05	0.16	0.04	0.16	8.52	62.81
cpy	0.03	0.08	0.25	0.01	0.02	7.17	8.75
cub	0.00	0.00	0.00	0.00	0.01	0.82	2.04

References

Adeyemi, Z., Holwell, D.A., Graham, S.D., Tordoff, B., 2016. Quantitative characterisation of low temperature hydrothermal alteration of magmatic Ni-Cu-PGE sulphide ores. Appl. Earth Sci. (Trans. Inst. Min. Metall. B) 125, 73.

Armitage, P.E.B., McDonald, I., Tredoux, M., 2007. A geological investigation of the Waterberg hydrothermal platinum deposit, Mookgophong, Limpopo Province, South Africa. Appl. Earth Sci. (Trans. Inst. Min. Metall. B) 116, 113–129.

Barkov, A.Y., Halkoaho, T.A.A., Kaajoki, K.V.O., Alapieti, T.T., Peura, R.A., 1997. Ruthenian pyrite and nickeloan malarite from the Imandra layered complex, northwestern Russia. Can. Mineral. 35, 887–897.

Barnes, S.J., Liu, W., 2012. Pt and Pd mobility in hydrothermal fluids: evidence from komatiites and from thermodynamic modelling. Ore Geol. Rev. 44, 49–58.

Barnes, S.J., Godel, B.M., Locmelis, M., Fiorentini, M.L., Ryan, C.G., 2011. Extremely Ni-rich Fe–Ni sulfide assemblages in komatiitic dunite at Betheno, Western Australia: results from synchrotron X-ray fluorescence mapping. Aust. J. Earth Sci. 58, 691–709.

Boudreau, A., Djon, L., Tchalikian, A., Corkery, J., 2014. The Lac Des Iles Palladium Deposit, Ontario, Canada part I. The effect of variable alteration on the Offset Zone. Miner. Deposita 49, 625–654.

Cafagna, F., Jugo, P.J., 2016. An experimental study on the geochemical behavior of highly siderophile elements (HSE) and metalloids (As, Se, Sb, Te, Bi) in a mss-iss-pyrite system at 650 °C: a possible magmatic origin for Co-HSE-bearing pyrite and the role of metalloid-rich phases in the fractionation of HSE. Geochim. Cosmochim. Acta 178, 233–258.

Capistrant, P.L., Hitzman, M.W., Wood, D., Kelly, N.M., Williams, G., Zimba, M., Kuiper, Y., Jack, D., Stein, H., 2015. Geology of the enterprise hydrothermal nickel deposit, North-Western Province, Zambia. Econ. Geol. 110, 9–38.

Cave, B.J., Stepanov, S., Craw, D., Large, R.R., Halpin, J.A., Thompson, J.M., 2015. Release of trace elements through the sub-greenschist facies breakdown of detrital rutile to metamorphic titanite in the Otago schist, New Zealand. Can. Mineral. 53, 379–400.

Cave, B.J., Pitcairn, I.K., Craw, D., Large, R.R., Thompson, J.M., Johnson, S.C., 2017. A metamorphic mineral source for tungsten in the turbidite-hosted orogenic gold deposits of the Otago Schist, New Zealand. Miner. Deposita 52, 515–537.

Coleman, R.G., Keith, T.E., 1971. A Chemical Study of Serpentinization—Burro Mountain, California. J. Petrol. 12, 311–328.

Craig, J.R., 1973. Pyrite-pentlandite assemblages and other low temperature relations in the Fe-Ni-S system. Am. J. Sci. 273-A, 496–510.

Craig, J.R., Kullurud, G., 1969. Phase relations in the Cu-Fe-Ni-S system and their application to magmatic ore deposits. Econ. Geol. Mon. 4, 344–358.

Dare, S.A.S., Barnes, S.J., Prichard, H.M., Fisher, P.C., 2011. Chalcophile and platinum-group element (PGE) concentrations in the sulfide minerals from the McCreedy East deposit, Sudbury, Canada, and the origin of PGE in pyrite. Miner. Deposita 46, 381–407.

Djon, M.L.N., Barnes, S.J., 2012. Changes in sulfides and platinum-group minerals with the degree of alteration in the Roby, twilight and high grade zones of the Lac-des-Iles complex, Ontario. Canada. Miner. Deposita 47, 875–896.

Duran, C.J., Barnes, S.-J., Corkery, J.T., 2015. Chalcophile and palladium-group element distribution in pyrites from the sulfide-rich pods of the Lad des Iles deposits, Western Ontario, Canada: implications for post-cumulus re-equilibration of the ore and the use of pyrite compositions in exploration. J. Geochem. Explor. 158, 223–242.

Duran, C.J., Barnes, S.-J., Corkery, J.T., 2016. Trace element distribution in primary sulfides and Fe–Ti oxides from the sulfide-rich pods of the Lac des Iles Pd deposits, Western Ontario, Canada: constraints on processes controlling the composition of the ore and the use of pentlandite compositions in exploration. J. Geochem. Explor. 166, 45–63.

Eales, H.V., Cawthorn, R.G., 1996. The Bushveld Complex. In: Cawthorn, R.G. (Ed.), Layered Intrusions. Elsevier Science, pp. 181–230.

Gervilla, F., Kojonen, K., 2002. The platinum-group minerals in the upper section of the Keivitsansarvi Ni-Cu-PGE deposit, northern Finland. Can. Mineral. 40, 377–394.

Giggenbach, W.F., 1988. Geothermal solute equilibria: derivation of Na-K-Mg-Ca geoindicators. Geochim. Cosmochim. Acta 52 (12), 2749–2765.

Giggenbach, W.F., 1997. The origin and evolution of fluids in magmatic-hydrothermal systems. In: Barnes, H.L. (Ed.), Geochemistry of Hydrothermal Ore Deposits, 3rd ed. John Wiley and Sons, pp. 737–796.

Godel, B., Barnes, S.-J., Maier, W.D., 2007. Platinum-group elements in sulphide minerals, platinum-group minerals, and whole-rocks of the Merensky Reef (Bushveld Complex, South Africa): implications for the formation of the reef. J. Petrol. 48, 1569–1604.

Goldfarb, R.J., Baker, T., Dubé, B., Groves, D.I., Hart, C.J.R., Gosselin, P., 2005. Distribution, character, and genesis of gold deposits in metamorphic terranes within Society of Economic Geologists. In: Hedenquist J.W. (eds) Economic geology 100th anniversary volume, 407–450.

González-Álvarez, I., Pirajno, F., Kerrich, R., 2013. Hydrothermal nickel deposits: secular variation and diversity. Ore Geol. Rev. 52, 1–3.

Graham, S.D., Holwell, D.A., McDonald, I., Jankin, G.R.T., Hill, N.J., Boyce, A.J., Smith, J., Sangster, C., 2017. Magmatic Cu-Ni-PGE-Au sulfide mineralisation in alkaline magmatic systems: an example from the Sron Garbh intrusion, Tyndrum, Scotland. Ore Geol. Rev. 80, 961–984.

Holland, T.J.B., Powell, R., 1998. An internally consistent thermodynamic data set for phases of petrological interest. J. Metamorph. Geol. 16 (3), 309–343.

Holwell, D.A., McDonald, I., 2007. Distribution of platinum-group elements in the Platreef at Overysel, northern Bushveld Complex: a combined PGM and LA-ICP-MS study. Contrib. Miner. Petrol. 154, 171–190.

Holwell, D.A., McDonald, I., 2010. A review of the behaviour of platinum group elements within natural magmatic sulfide ore systems. Platinum Met. Rev. 54, 26–36.

Holwell, D.A., Keays, R.R., Firth, E.A., Findlay, J., 2014. Geochemistry and mineralogy of platinum-group element mineralisation in the River Valley intrusion, Ontario, Canada: a model for early stage S saturation and multi stage emplacement and the implications for 'contact-type' Ni-Cu-PGE mineralisation. Econ. Geol. 109, 689–712.

Hulbert, L.J., 1983. A Petrographical Investigation of the Rustenburg Layered Suite and Associated Mineralization South of Potgietersrus. (Unpublished D.Sc. Dissertation) The University of Pretoria, Pretoria, South Africa.

Hulbert, L.J., von Gruenewaldt, G., 1982. Nickel, copper and platinum mineralization in the Lower Zone of the Bushveld Complex, south of Potgietersrus'. Econom. Geol. 77, 1296.

Hulbert, L.J., Duke, J.M., Eckstrand, O.R., Lydon, J.W., Scoates, R.F.J., Cabri, L.J., 1988. Geological environments of the platinum group elements. Geological Survey of Canada Open File Report 1440, 1–148.

Hutchinson, D., Kinnaird, J.A., 2005. Complex multistage genesis for the Ni–Cu–PGE mineralization in the southern region of the Platreef, Bushveld Complex, South Africa. Appl. Earth Sci. 114, B208–B223.

Johnson, J.W., Oelkers, E.H., Helgeson, H.C., 1992. Supcrt92 – a software package for calculating the standard molal thermodynamic properties of minerals, gases, aqueous species, and reactions from 1 bar to 5000 bar and 0 °C to 1000 °C. Comput. Geosci. 18 (7), 899–947.

Keays, R.R., Jowitt, S.M., 2013. The Avebury Ni deposit, Tasmania; a case study of an unconventional Nickel deposit. Ore Geol. Rev. 52, 4–17.

Klemd, R., Herderich, T., Junge, M., Oberthür, T., Schouwstra, R., Roberts, J., 2016. Platinum-group element concentrations in base-metal sulphides from the Platreef, Mogalakwena Platinum Mine, Bushveld Complex, South Africa. S. Afr. J. Geol. 119, 623–638.

Kullerud, G., Yund, R.A., Moh, G.H., 1969. Phase relations in the Cu-Fe-S, Cu-Ni-S, and Fe-Ni-S systems. Econ. Geol. Monogr. 4, 323–343.

Le Vaillant, M., Barnes, S.J., Fiorentini, M.L., Miller, J., McCaig, T.C., Muccili, P., 2015. A hydrothermal Ni-As-PGE geochemical halo around the Miitel komatiite-hosted nickel sulfide deposit, Yilgarn Craton, Western Australia. Econ. Geol. 110, 505–530.

Le Vaillant, M., Saleem, A., Barnes, S.J., Fiorentini, M.L., Miller, J., Beresford, S., Perring, C., 2016a. Hydrothermal remobilisation around a deformed and remobilised komatiite-hosted Ni-Cu-(PGE) deposit, Sarah's Find, Agnew Wiluna greenstone belt, Yilgarn Craton, Western Australia. Mineral. Deposita 51, 288–369.

Le Vaillant, M., Barnes, S.J., Fiorentini, M.L., Santaguida, F., Törmänen, T., 2016b. Effects of hydrous alteration on the distribution of base metals and platinum group elements within the Kevitsa magmatic nickel sulphide deposit. Ore Geol. Rev. 72, 128–148.

Li, C., Ripley, E.M., Merino, E., Maier, W.D., 2004. Replacement of base metal sulphides by actinolite, epidote, calcite and magnetite in the UG2 and Merensky Reef of the Bushveld Complex, South Africa. Econ. Geol. 99, 173–184.

Liu, W., McPhail, D.C., 2005. Thermodynamic properties of copper chloride complexes and copper transport in magmatic-hydrothermal solutions. Chem. Geol. 221, 21–39.

Liu, W., Migdisov, A., Williams-Jones, A., 2012. The stability of aqueous nickel(II) chloride complexes in hydrothermal solutions: results of UV–visible spectroscopic experiments. Geochim. Cosmochim. Acta 94, 276–290.

Loukola-Ruskeeniemi, K., Lahtinen, H., 2013. Multiphase evolution in the black-shale hosted Ni–Cu–Zn–Co deposit at Talvivaara, Finland. Ore Geol. Rev. 52, 85–99.

McDonald, I., Holwell, D.A., 2011. Geology of the Northern Bushveld Complex and the Setting and Genesis of the Platreef Ni-Cu-PGE Deposit. Rev. Econ. Geol. 17, 297–327.

McDonald, I., Tredoux, M., Vaughan, D.J., 1995. Platinum mineralization in quartz veins near Naboomspruit, central Transvaal, South African. J. Geol. 98, 168–175.

McDonald, I., Ohnenstetter, D., Rowe, J.P., Tredoux, M., Pattrick, R.A.D., Vaughan, D.J., 1999. Platinum precipitation in the Waterberg deposit, Naboomspruit, South Africa. S. Afr. J. Geol. 102, 184–191.

Misra, K.C., Fleet, M.E., 1974. Chemical composition and stability of violarite. Econ. Geol. 59, 391–403.

Mountain, B.W., Wood, S.A., 1988. Chemical controls on the solubility, transport, and deposition of platinum and palladium in hydrothermal solutions: a thermodynamic approach. Econ. Geol. 83, 492–510.

Naldrett, A.J., 2011. Fundamentals of magmatic sulfide deposits. In: Li, C., Ripley, E.M. (Eds.), Magmatic Ni-Cu and PGE deposits: Geology, Geochemistry, and Genesis. Society of Economic Geology. Rev. Econ. Geol. 17. pp. 1–50.

Naldrett, A.J., Kullerud, G., 1967. A study of the Strathcona mine and its bearing on the origin of the nickel-copper ores of the Sudbury District, Ontario. J. Petrol. 8, 453–531.

Naldrett, A.J., Craig, J.R., Kullerud, G., 1967. The central portion of the Fe-Ni-S system and its bearing on pentlandite exsolution in iron-nickel sulfide ores. Econ. Geol. 62, 826–847.

Nyman, M.W., Sheets, R.W., Bodnar, R.J., 1990. Fluid-inclusion evidence for the physical and chemical conditions associated with intermediate-temperature PGE mineralization at the New Rambler Deposit, southeastern Wyoming. Can. Mineral. 28, 629–638.

Oberthür, T., Cabri, L.J., Weiser, T.W., McMahon, G., 1997. Pt, Pd and other trace elements in sulfides of the main sulfide zone, Great Dike, Zimbabwe: a reconnaissance study. Can. Mineral. 35, 597–609.

Osbahr, I., Klemd, R., Oberthür, T., Brätz, H., Schouwstra, R., 2013. Platinum-group element distribution in base-metal sulfides of the Merensky Reef from the eastern and western Bushveld Complex, South Africa. Mineral. Deposita 48, 211–232.

Patten, C., Pitcairn, I., Teagle, D.A.H., Harris, M., 2016. Mobility of Au and related elements during the hydrothermal alteration of the oceanic crust: implications for the sources of metals in VMS deposits. Miner. Deposita 51, 179–200.

Piña, R., Gervilla, F., Barnes, S.J., Ortega, L., Lunar, R., 2012. Distribution of platinum-group and chalcophile elements in the Aguablanca Ni–Cu sulfide deposit (SW Spain): evidence from a LA-ICP-MS study. Chem. Geol. 302–303, 61–75.

Piña, R., Gervilla, F., Barnes, S.J., Ortega, L., Lunar, R., 2013. Platinum-group elements-

bearing pyrite from the Aguablanca Ni-Cu sulphide deposit (SW Spain): a LA-ICP-MS study. Eur. J. Mineral. 25, 241–252.

Piña, R., Gervilla, F., Barnes, S.-J., Oberthür, T., 2016. Platinum-group element concentrations in pyrite from the Main Sulfide Zone of the Great Dyke of Zimbabwe. Miner. Deposita 51, 853–872.

Pirajno, F., González-Álvarez, I., 2013. A re-appraisal of the Epoch nickel sulphide deposit, Filabusi Greenstone Belt, Zimbabwe: a hydrothermal nickel mineral system? Ore Geol. Rev. 52, 58–65.

Pitcairn, I.K., Teagle, D.A.H., Craw, D., Olivo, G.R., Kerrich, R., Brewer, T.S., 2006. Sources of metals and fluids in orogenic gold deposits: insights from the Otago and Alpine schists, New Zealand. Econ. Geol. 101, 1525–1546.

Pitcairn, I.K., Olivo, G.R., Teagle, D.A.H., Craw, D., 2010. Sulfide evolution during prograde metamorphism of the Otago and Alpine Schists, New Zealand. Can. Mineral. 48, 1267–1295.

Prichard, H.M., Knight, R.D., Fisher, P.C., McDonald, I., Zhou, M.-F., Wang, C.Y., 2013. Distribution of platinum-group elements in magmatic and altered ores in the Jinchuan intrusion, China: an example of selenium remobilization by post magmatic fluids. Miner. Deposita 48, 767–786.

Reed, M., Palandri, J., 2013. SOLTHERM.H08: a database of equilibrium constants for minerals and aqueous species. University of Oregon, Eugene, OR.

Reed, M.H., 1982. Calculation of multicomponent chemical equilibria and reaction processes in systems involving minerals, gases and an aqueous phase. Geochim. Cosmochim. Acta 46 (4), 513–528.

Reed, M.H., 1997. Hyodrothermal alteration and its relationship to ore fluid composition. In: Barnes, H.L. (Ed.), Geochemistry of Hydrothermal Ore Deposits. Volume 1, pp. 303–365.

Reed, M.H., 1998. Calculation of simultaneous chemical equilibria in aqueous-mineral-gas systems and its application to modeling hydrothermal processes. In: Richards, J., Larson, P. (Eds.), Techniques in Hydrothermal Ore Deposits Geology. Reviews in Economic Geology. Society of Economic Geologists, pp. 109–124.

Sener, A.K., Grainger, C.J., Groves, D.J., 2002. Epigenetic gold platinum-group element deposits: examples from Brazil and Australia. Appl. Earth Sci. (Trans. Inst. Min. Metall. Sect. B) 101B, B65–B72.

Shock, E.L., 2007. An updated and augmented version (slop07.dat) of the original SUPCRT92 database (sprons92.dat).

Smith, J.W., 2014. The nature and origin of PGE mineralization in the Rooipoort area, northern Bushveld Complex, South Africa. (Unpublished PhD thesis) University of Leicester, UK.

Smith, J.W., Holwell, D.A., McDonald, I., 2011. The mineralogy and petrology of platinum-group element-bearing sulphide mineralization within the Grasvally Norite-Pyroxenite-Anorthosite (GNPA) member, south ofMokopane, northern Bushveld Complex, South Africa. Appl. Earth Sci. (Trans. Inst. Min. Metall. B) 120, B158–B174.

Smith, J.W., Holwell, D.A., McDonald, I., 2014. Precious and base metal geochemistry and mineralogy of the Grasvally Norite-Pyroxenite-Anorthosite (GNPA) member, northern Bushveld Complex, South Africa: implications for a multistage emplacement. Miner. Deposita 49, 667–692.

Smith, J.W., Holwell, D.A., McDonald, I., Boyce, A.J., 2016. The application of S isotopes and S/Se ratios in determining ore-forming processes of magmatic Ni–Cu–PGE sulfide deposits: a cautionary case study from the northern Bushveld Complex. Ore Geol. Rev. 73, 148–174.

Smith, D.J., Naden, J., Jenkin, G.R.T., Keith, M., 2017. Hydrothermal alteration and fluid pH in alkaline-hosted epithermal systems. Ore Geol. Rev. http://dx.doi.org/10.1016/j.oregeorev.2017.06.028.

Sutherland, A.J., Holwell, D.A., Smith, J.W., 2012. The nature and genesis of PGE-rich sulphide horizons on the farm War Springs, northern Bushveld Complex, South Africa. Appl. Earth Sci. (Trans. Inst. Min. Metall. B) 121, 209–210.

Wood, S.A., 2002. The aqueous geochemistry of the platinum-group elements with applications to ore deposits. In: Cabri, L.J. (Ed.), The Geology, Geochemistry, Mineralogy and Mineral Beneficiation of Platinum-Group Elements. Special Volume 54. Canadian Institute of Mining, Metallurgy and Petroleum, pp. 211–249.

Yund, R.A., Kullerud, G., 1966. Thermal stability assemblages in the Cu-Fe-S system. J. Pterol. 7, 454–488.